

ON THE MAXIMUM LUMINOSITY OF GALAXIES AND THEIR CENTRAL BLACK HOLES: FEEDBACK FROM MOMENTUM-DRIVEN WINDS

NORMAN MURRAY,^{1,2,3} ELIOT QUATAERT,⁴ AND TODD A. THOMPSON^{4,5}

Received 2004 May 24; accepted 2004 September 20

ABSTRACT

We investigate large-scale galactic winds driven by momentum deposition. Momentum injection is provided by (1) radiation pressure produced by the continuum absorption and scattering of photons on dust grains and (2) supernovae (momentum injection by supernovae is important even if the supernova energy is radiated away). Radiation can be produced by a starburst or active galactic nucleus (AGN) activity. We argue that momentum-driven winds are an efficient mechanism for feedback during the formation of galaxies. We show that above a limiting luminosity, momentum deposition from star formation can expel a significant fraction of the gas in a galaxy. The limiting, Eddington-like luminosity is $L_M \simeq (4f_g c/G)\sigma^4$, where σ is the galaxy velocity dispersion and f_g is the gas fraction; the subscript M refers to momentum driving. A starburst that attains L_M moderates its star formation rate and its luminosity does not increase significantly further. We argue that elliptical galaxies attain this limit during their growth at $z \gtrsim 1$ and that this is the origin of the Faber-Jackson relation. We show that Lyman break galaxies and ultraluminous infrared galaxies have luminosities near L_M . Since these starbursting galaxies account for a significant fraction of the star formation at $z \gtrsim 1$, this supports our hypothesis that much of the observed stellar mass in early-type galaxies was formed during Eddington-limited star formation. Star formation is unlikely to efficiently remove gas from very small scales in galactic nuclei, i.e., scales much smaller than that of a nuclear starburst. This gas is available to fuel a central black hole (BH). We argue that a BH clears gas out of its galactic nucleus when the luminosity of the BH itself reaches $\approx L_M$. This shuts off the fuel supply to the BH and may also terminate star formation in the surrounding galaxy. As a result, the BH mass is fixed to be $M_{\text{BH}} \simeq (f_g \kappa_{\text{es}}/\pi G^2)\sigma^4$, where κ_{es} is the electron scattering opacity. This limit is in accord with the observed $M_{\text{BH}}-\sigma$ relation.

Subject headings: galaxies: formation — galaxies: fundamental parameters — galaxies: general — galaxies: starburst — intergalactic medium

Online material: color figures

1. INTRODUCTION

Large elliptical galaxies in the local universe exhibit a relation between their luminosity L and the depth of their gravitational potential wells (as measured by their stellar velocity dispersion σ) of the form $L \propto \sigma^4$, a result first noted nearly 30 years ago (Faber & Jackson 1976). More recently it was found that most nearby early-type galaxies (elliptical galaxies and spiral bulges) contain massive black holes (BHs) and that the mass M_{BH} of the hole scales as $M_{\text{BH}} \propto \sigma^4$ (Ferrarese & Merritt 2000; Gebhardt et al. 2000; Tremaine et al. 2002). If these BHs radiate near their Eddington limit, their luminosity would also satisfy $L \propto \sigma^4$. It would be remarkable if this correspondence with the Faber-Jackson (FJ) relation is a coincidence.

In an apparently unrelated phenomenon, nearby starburst galaxies, which are generally spiral galaxies but also include dwarf irregulars and dwarf elliptical galaxies, are seen to drive large-scale galactic outflows (Heckman et al. 1990; Martin 1999; Heckman 2000; Strickland 2004; Martin 2004). More distant starburst galaxies include Lyman break galaxies (LBGs; Steidel et al. 1996) and SCUBA sources (e.g., Smail et al. 1997).

These also show evidence for large-scale outflows (e.g., Pettini et al. 2000; Adelberger et al. 2003). The SCUBA sources have infrared luminosities as large as $10^{13} L_{\odot}$, making them ultraluminous infrared galaxies (ULIRGs; e.g., Genzel & Cesarsky 2000). The space density and mass of the ULIRGs suggest that they are the progenitors of present-day massive elliptical galaxies.

In this article we argue that all of these phenomena are intimately related; they result directly from a limit on the luminosity of massive self-gravitating gas-rich objects set by momentum deposition in the interstellar medium. We show that significant momentum injection into the interstellar medium (ISM) of star-forming galaxies may be accomplished by two sources: radiation pressure from the continuum absorption and scattering of photons on dust grains, and supernovae (SNe).⁶ The photons may come from either the starburst itself or a central massive BH. SNe have often been considered as an energy source for thermal pressure-driven galactic winds. Less consideration has been given to SNe as a source of momentum flux into the ISM; unlike energy, the momentum SN deposit cannot be radiated away.

Starburst galaxies both locally and at high redshift are typically highly reddened (e.g., Heckman et al. 1990; Meurer et al. 1995; Sanders & Mirabel 1996; Adelberger & Steidel 2000; Calzetti 2001; Genzel et al. 2004). Optical depths to UV/IR

¹ Canadian Institute for Theoretical Astrophysics, University of Toronto, 60 St. George Street, Toronto, ON M5S 3H8, Canada; murray@cita.utoronto.ca.

² Canada Research Chair in Astrophysics.

³ Visiting Miller Professor, University of California, Berkeley.

⁴ Astronomy Department and Theoretical Astrophysics Center, University of California, 601 Campbell Hall, Berkeley, CA 94720; eliot@astro.berkeley.edu, thomp@astro.berkeley.edu.

⁵ Hubble Fellow.

⁶ Haehnelt (1995) also considered some properties of feedback by momentum deposition during galaxy formation, focusing on radiation pressure from Lyman edge photons, rather than dust or SNe.

photons may easily exceed unity, suggesting that a large fraction of the momentum created by star formation is available to drive an outflow. As noted above, a central active galactic nucleus (AGN) provides an alternative source of photons. We show that either source can drive a galactic wind. Previous authors have considered the possibility that dust itself is expelled from galaxies by radiation pressure, particularly in the context of enriching the intergalactic medium (IGM) with metals (Davies et al. 1998; Aguirre 1999; Aguirre et al. 2001a, 2001b, 2001c). We argue that, as in models of dust-driven stellar winds (e.g., Netzer & Elitzur 1993), the dust and gas are hydrodynamically coupled and thus that the dust can drag the gas out of the galaxy.

This paper is organized as follows. We begin by considering the general properties of momentum-driven galactic winds in § 2.2. We show via an Eddington-like argument that there exists a limiting starburst luminosity above which a large fraction of the gas in a galaxy can be expelled. When the gas is optically thick, the limiting luminosity is given by

$$L_M = \frac{4f_g c}{G} \sigma^4, \quad (1)$$

where f_g is the fraction of mass in gas.⁷ Scoville (2003) has considered an analogous optically thin Eddington limit in setting the maximum luminosity per unit mass in star-forming galaxies. In § 3 we contrast the properties of momentum-driven winds with those of energy-driven winds that are more typically invoked in the galactic context (Chevalier & Clegg 1985; Heckman et al. 1990). We also show that the dynamics of cold gas entrained in a hot thermal wind is analogous to that of the momentum-driven outflows considered in § 2 (we elaborate on this point in the Appendix).

With equation (1) in hand, we focus on the importance of this limit for setting the observed properties of elliptical galaxies. In § 4 we present observational evidence that the star formation rates required to reach our limiting luminosity are realized during the formation of massive galaxies at high redshift. These high star formation rates are probably initiated by galaxy mergers. It follows that star formation in elliptical galaxies self-regulates via momentum deposition. We show that this model can account for the FJ relation between the current luminosity and velocity dispersion of early-type galaxies.

We also summarize data showing that the most luminous galaxies at any σ and redshift, not just massive elliptical galaxies, roughly satisfy equation (1). We argue that this implies that energy deposition by SNe is not efficient at globally halting star formation, even in small galaxies. This is in contrast to the conventional picture in the galaxy formation literature (Dekel & Silk 1986).

We then consider the relative role of AGNs and star formation in driving large-scale galactic winds (§ 5). We provide observational evidence that the most luminous AGNs have luminosities $\approx L_M$. This supports a model in which accretion onto AGNs self-regulates in a manner similar to that of star formation on galactic scales. When the AGN luminosity (and BH mass) exceeds a critical value, the AGN clears gas out of the galactic nucleus, shutting off its own fuel supply. This can account for the observed $M_{\text{BH}}-\sigma$ relation. Our treatment of self-regulated BH growth is similar to that of King (2003; see also

Silk & Rees 1998; Haehnelt et al. 1998; Blandford 1999; Fabian 1999; Fabian et al. 2002).

Finally, in § 6 we summarize our results and discuss further implications of momentum-driven galactic winds.

2. MOMENTUM-DRIVEN GALACTIC WINDS

In this section we review the basics of momentum-driven winds. In § 3 we contrast the scalings derived here for momentum deposition with the corresponding relations for energy-driven galactic outflows.

2.1. Preliminaries

We take as a model for the gravitational potential that of an isothermal sphere with gas density and mass profiles given by

$$\rho(r) = \frac{f_g \sigma^2}{2\pi G r^2} \quad (2)$$

and

$$M_g(r) = \frac{2f_g \sigma^2 r}{G}, \quad (3)$$

where σ is the velocity dispersion and f_g is the gas fraction. We assume that f_g is a constant throughout this work.

The goal of this paper is both to elucidate the physics of momentum-driven galactic winds and to discuss the applicability of such outflows to rapidly star-forming galaxies at high redshift. For the latter purpose, it is convenient to consider several physical scales characterizing galaxies. We follow the treatment of Mo et al. (1998). The virial radius of the dark matter halo is given by

$$R_V = \sqrt{2}\sigma/[10H(z)] \sim 285\sigma_{200}h^{-1}[H_0/H(z)] \text{ kpc}, \quad (4)$$

where $H(z)$ is the Hubble constant at redshift z where the halo is formed, $H_0 = 100 h \text{ km s}^{-1} \text{ Mpc}^{-1}$, and $\sigma_{200} = \sigma/200 \text{ km s}^{-1}$. The dynamical timescale on the scale R_V is

$$\tau_{\text{dyn}}^V = R_V/\sigma \sim 1.4h^{-1}[H_0/H(z)] \text{ Gyr}. \quad (5)$$

The total gas mass within a dark matter halo of dispersion σ is $\approx M_g(R_V)$. Using equation (3), this yields

$$M_g = 5 \times 10^{11} f_{g,0.1} \sigma_{200}^3 h^{-1} [H_0/H(z)] M_\odot, \quad (6)$$

where $f_{g,0.1} = f_g/0.1$.

Although the mass in dark matter is distributed out to the virial radius R_V , the baryons cool and condense in the dark matter halo and are thus significantly concentrated with respect to the dark matter. The “disk” radius characterizing the baryons is related to the virial radius by

$$R_D = \frac{1}{\sqrt{2}} \lambda R_V \sim 10\lambda_{0.05}\sigma_{200}h^{-1}[H_0/H(z)] \text{ kpc}, \quad (7)$$

where $\lambda_{0.05} = \lambda/0.05$ is the spin parameter of the dark matter halo (Bullock et al. 2001). The dynamical timescale on the scale R_D is then

$$\tau_{\text{dyn}}^D = R_D/\sigma \sim 50\lambda_{0.05}h^{-1}[H_0/H(z)] \text{ Myr}. \quad (8)$$

⁷ A potentially related empirical limit on the surface brightness of starburst galaxies has been described by Meurer et al. (1997).

Note that both τ_{dyn}^V and τ_{dyn}^D are independent of σ and are fixed fractions of the Hubble time, $H(z)^{-1}$.

There is a final length scale and timescale that is not easily deduced from parameters of the dark matter, namely, that characterizing a starburst. Observations of systems ranging from local dwarf starbursts to ULIRGs at high redshift show that star formation can be distributed on scales ranging from ~ 100 pc to several kiloparsecs. It is important to note that although the dynamical time of the starburst region might be rather short (e.g., ≈ 5 Myr for a nuclear burst on kiloparsec scales), the duration of the star formation activity ($\equiv \tau_{\text{SB}}$) can be significantly longer. In particular, for starbursts triggered by a major merger, the duration of the burst may be set by the duration of the merger, which is several dynamical times τ_{dyn}^D (eq. [8]).

2.2. Momentum Injection and the Mass-Loss Rate

The maximal mass-loss rate \dot{M}_W of a momentum-driven outflow from an object with total momentum deposition rate \dot{P} is given by

$$\dot{M}_W V_\infty \approx \dot{P}, \quad (9)$$

where V_∞ is the terminal velocity of the wind. We show below that for galaxies $V_\infty \sim \sigma$. We consider two primary sources of momentum deposition in driving large-scale galactic outflows: SNe and radiation pressure from the central starburst or AGN. In the former case, assuming that each SN produces $\approx 10 M_\odot$ of material moving at $v \approx 3000$ km s $^{-1}$, we estimate a net momentum deposition rate of

$$\dot{P}_{\text{SN}} \sim 2 \times 10^{33} \left(\frac{\dot{M}_*}{1 M_\odot \text{ yr}^{-1}} \right) \text{ g cm s}^{-2}, \quad (10)$$

where \dot{M}_* is the star formation rate and we assume one SN per 100 yr per $M_\odot \text{ yr}^{-1}$ of star formation.⁸ This momentum deposition by SNe occurs even if the kinetic energy of the explosion is efficiently radiated away. Note also that winds from massive stars can provide a momentum flux comparable to that provided by SNe (Leitherer et al. 1999).

In the case of radiation pressure from a nuclear starburst or AGN, in the point-source, single-scattering limit, $\dot{P} = L/c$, where L is the luminosity of the central radiating object and L/c is the total momentum flux. Although both a starburst and an AGN may contribute to the galaxy luminosity, we consider only the starburst contribution to the total luminosity (L_{SB}) in this section. We explore the role of AGNs in § 5.

We can compare \dot{P}_{SN} with L_{SB}/c for the starburst by writing $L_{\text{SB}} = \epsilon \dot{M}_* c^2$. Examination of the starburst models of Leitherer et al. (1999) and Bruzual & Charlot (2003) indicates that for a Salpeter initial mass function (IMF),⁹ $\epsilon \sim 10^{-3} \equiv \epsilon_3$, or that

$$L_{\text{SB}}/c \sim 2 \times 10^{33} \epsilon_3 \left(\frac{\dot{M}_*}{1 M_\odot \text{ yr}^{-1}} \right) \text{ g cm s}^{-2}. \quad (11)$$

⁸ Shell-shell collisions in a spatially homogeneous distribution of SN remnants will cancel momentum at shell-shell interfaces. Hence, only outside the region where the distribution can be described as homogeneous will there be a significant outward radial momentum flux. Therefore, the estimate of eq. (10) should be regarded as an upper limit to the net momentum injection available for driving a wind.

⁹ The efficiency ϵ depends on the low-mass cutoff of the IMF, m_l , as $\epsilon \propto m_l^{0.35}$.

Comparing equations (10) and (11), we see that the net momentum deposited by SN explosions is roughly the same as that deposited by stars. With this in mind, we write equation (9) as

$$\dot{M}_W V_\infty \approx L_{\text{SB}}/c. \quad (12)$$

If the driving mechanism is pure radiation pressure from a central starburst or AGN, this equality is only appropriate if the flow has optical depth (τ) of order unity. More generally, given an optical depth τ , “ $\tau L/c$ ” replaces “ L/c .”

Since both \dot{P}_{SN} and L_{SB} are proportional to the star formation rate \dot{M}_* , equation (12) immediately implies that in a momentum-driven galactic wind the mass-loss rate is proportional to the star formation rate:

$$\dot{M}_W \sim \dot{M}_* \left(\frac{\epsilon c}{V_\infty} \right) = \dot{M}_* \left(\frac{300 \epsilon_3 \text{ km s}^{-1}}{V_\infty} \right). \quad (13)$$

This implies that, for $V_\infty \sim \sigma \sim 200$ km s $^{-1}$, $\dot{M}_W \sim \dot{M}_*$.

2.3. Wind Dynamics: Optically Thick Limit

We approximate the gas surrounding a point source with luminosity L as a spherical optically thick shell. Ignoring gas pressure, the momentum equation for the gas can be written as

$$\frac{dP}{dt} = M_g(r) \frac{dV}{dt} = -\frac{GM(r)M_g(r)}{r^2} + \frac{L(t)}{c}. \quad (14)$$

Using equation (3), we see that if $L(t)$ is less than the critical luminosity

$$L_M = \frac{4f_g c}{G} \sigma^4, \quad (15)$$

where the subscript “ M ” on the limiting luminosity L_M stands for “momentum-driven,” then the effective gravity is reduced by the momentum deposition of the radiation, but the motion of the gas is inward toward the central point source. For $L \gtrsim L_M$, the gas moves outward in a radiation pressure–driven outflow. Taking $L(t)$ constant in time in equation (14) implies

$$\frac{dV}{dt} = \frac{GM(r)}{r^2} \left(\frac{L}{L_M} - 1 \right) = \frac{2\sigma^2}{r} \left(\frac{L}{L_M} - 1 \right). \quad (16)$$

Taking equation (16) as the momentum equation for a time-independent optically thick wind (not a shell) and integrating, we obtain

$$V(r) = 2\sigma \sqrt{\left(\frac{L}{L_M} - 1 \right) \ln \left(\frac{r}{R_0} \right)}, \quad (17)$$

where R_0 is the initial radius of the outflow and we have neglected $V(R_0)$. For L of a few times L_M and distances as large as several $R_V (\gg R_0)$, the asymptotic velocity does not exceed several times σ , i.e., $V_\infty \approx 3\sigma$.

When $L \gtrsim L_M$, the momentum injected by star formation is sufficient to blow out *all* of the gas in the galaxy. Taking $f_{9.01} = f_g/0.1$ and $\sigma_{200} = \sigma/200$ km s $^{-1}$ yields

$$L_M \simeq 3 \times 10^{46} f_{9.01} \sigma_{200}^4 \text{ ergs s}^{-1}. \quad (18)$$

The star formation rate corresponding to L_M is then

$$\dot{M}_* = L_M / \epsilon c^2 \simeq 500 f_{g,0.1} \epsilon_3^{-1} \sigma_{200}^4 M_\odot \text{ yr}^{-1}. \quad (19)$$

From equation (12), the outflow rate is

$$\dot{M}_W \simeq 500 f_{g,0.1} \sigma_{200}^3 M_\odot \text{ yr}^{-1}. \quad (20)$$

Equations (15) and (20) imply that $\dot{M}_W \propto \sigma^3 \propto L^{3/4}$.

It is worth considering whether the luminosity L_M can plausibly be obtained in a starburst. In § 4 we provide observational evidence that it is, while here we present a simple theoretical estimate. The maximum star formation rate in a dark matter potential well can be estimated by first assuming that the gas builds up on a scale $\sim R_D$ without much star formation, as in Mo et al. (1998). Mergers and interactions between galaxies can then efficiently convert this gas into stars on a timescale $\sim \tau_{\text{dyn}}^D \sim R_D / \sigma$, the merger timescale. This can in principle generate a star formation rate approaching

$$\dot{M}_*^{\text{max}} = \frac{M_g}{\tau_{\text{DYN}}^D} = \frac{2^{3/2} f_g}{\lambda G} \sigma^3 \sim 10^4 f_{g,0.1} \lambda_{0.05}^{-1} \sigma_{200}^3 M_\odot \text{ yr}^{-1}, \quad (21)$$

producing a maximum luminosity of

$$L_{\text{max}} = \epsilon \dot{M}_*^{\text{max}} c^2 \sim 6 \times 10^{47} \epsilon_3 f_{g,0.1} \lambda_{0.05}^{-1} \sigma_{200}^3 \text{ ergs s}^{-1}. \quad (22)$$

With this estimate for the maximum star formation rate, there is a critical $\sigma \equiv \sigma_{\text{max}}$ above which a starburst cannot generate the luminosity required to expel the gas (i.e., $L_{\text{max}} \lesssim L_M$):

$$\sigma_{\text{max}} = \frac{\epsilon c}{\sqrt{2} \lambda} \sim 4000 \epsilon_3 \lambda_{0.05}^{-1} \text{ km s}^{-1}. \quad (23)$$

This estimate suggests that star formation rates required to produce a luminosity $\sim L_M$ can plausibly be achieved, particularly in mergers when stored gas is converted into stars on a timescale $\sim \tau_{\text{dyn}}^D$. The actual value of σ_{max} is, of course, quite uncertain because it depends on the efficiency of star formation and ambiguities in defining the dynamical timescale for the starburst. Equation (23) may well be an overestimate because the gas mass available for star formation at any time may be significantly less than the total mass M_g in equation (6).

2.4. Wind Dynamics: Optically Thin Limit

So far we have assumed that the flow is optically thick at the base of the wind. This is certainly appropriate in the case of pure momentum driving by SNe (\dot{P}_{SN}). However, if \dot{P} is provided by the luminosity of the starburst or AGN, then we must distinguish between the optically thick and optically thin limits. If the spherical shell surrounding a point source with luminosity L is optically thin, again ignoring gas pressure, the momentum equation for the shell is

$$\frac{dV}{dt} = -\frac{GM(r)}{r^2} + \frac{\kappa L}{4\pi r^2 c}, \quad (24)$$

where the optical depth $\tau = \kappa M_g(r) / 4\pi r^2$ and κ is the opacity (per unit mass of gas). Thus, the condition on the luminosity

for the shell to move outward is the classical (optically thin) Eddington result,

$$L_{\text{SB}} \gtrsim L_{\text{Edd}} = \frac{4\pi GM(r)c}{\kappa} = \frac{8\pi c}{\kappa} \sigma^2 r \\ \approx 10^{46} \sigma_{200}^2 r_{\text{kpc}} \kappa_{100}^{-1} \text{ ergs s}^{-1}, \quad (25)$$

where $\kappa_{100} = \kappa / 100 \text{ cm}^2 \text{ g}^{-1}$ and $r_{\text{kpc}} = r / 1 \text{ kpc}$. The velocity profile for a steady state optically thin wind can be obtained by integrating equation (24),

$$V(r) = 2\sigma \sqrt{R_g \left(\frac{1}{R_0} - \frac{1}{r} \right) + \ln \left(\frac{R_0}{r} \right)}, \quad (26)$$

where

$$R_g \equiv \frac{\kappa L}{8\pi c \sigma^2} = \frac{L}{L_{\text{Edd}}(R_0)} R_0. \quad (27)$$

The gas, close to R_0 , initially accelerates. When it reaches R_g , it begins to decelerate, eventually stopping if the galaxy is much larger than the initial launch radius R_0 . In order for the gas to reach 10 times its initial radius, we require $L/L_{\text{Edd}} \sim 3$.

Equations (24)–(27) also apply to optically thick *clouds* that fill only a fraction of the volume in the galaxy (in contrast to the optically thick *shell* considered in § 2.3). For a cloud of mass M_c and area A_c , the force per unit mass a distance r from the luminosity source is $A_c L / (4\pi r^2 c M_c)$. This is identical to the force in equation (24) with $\kappa \rightarrow A_c / M_c$. In this case the Eddington limit can be rewritten as

$$L_{\text{Edd}} \approx 2 \times 10^{45} \sigma_{200}^2 r_{\text{kpc}} N_{21} \text{ ergs s}^{-1}, \quad (28)$$

where $N_{21} = N_{\text{H}} / 10^{21} \text{ cm}^2$ is the hydrogen column and we have rewritten the mass per unit area of the cloud as $M_c / A_c = (4/3) m_p N_{\text{H}}$. More properties of the acceleration of optically thick clouds are considered in § 3.1 and the Appendix.

2.5. The Critical Opacity and Dust Production

The difference between the limiting luminosity derived in the optically thick case (L_M ; eq. [15]) and that derived in the optically thin case (L_{Edd} ; eq. [25]) is important. The dividing line between these physical regimes is given by a critical opacity κ_{crit} above which the gas is optically thick. To estimate κ_{crit} , we assume that all of the gas in a galaxy is concentrated on the scale R_D (see eq. [7]). The condition $\tau \gtrsim 1$ then requires $\kappa \gtrsim \kappa_{\text{crit}}$ with

$$\kappa_{\text{crit}} \approx \frac{\pi G \lambda^2}{\sqrt{2} \sigma f_g 10 H(z)} \simeq 6 \lambda_{0.05}^2 \sigma_{200}^{-1} f_{g,0.1}^{-1} h^{-1} \frac{H_0}{H(z)} \text{ cm}^2 \text{ g}^{-1}. \quad (29)$$

Note that this estimate applies both if the gas is distributed spherically on a scale $\sim R_D$ and if it is in a disk (τ is then the vertical optical depth through the disk). If $\kappa < \kappa_{\text{crit}}$ (particularly likely at lower redshift where $f_g \ll 0.1$ or in a small galaxy with $\sigma_{200} \ll 1$), then the optically thin limit obtains (eq. [25]). Conversely, if $\kappa > \kappa_{\text{crit}}$, then the optically thick limit obtains and the limiting luminosity required to drive the gas mass to infinity via momentum deposition is given by equation (15).

The critical opacity obtained in equation (29) is much larger than the electron scattering opacity ($\kappa_{\text{es}} \simeq 0.38 \text{ cm}^2 \text{ g}^{-1}$), but it is easily provided by continuum dust absorption and scattering of photons (e.g., Draine & Lee 1984). Dust opacity can be in the range of several hundred $\text{cm}^2 \text{ g}^{-1}$ and is responsible for the high reddening observed in both local (e.g., Calzetti 2001; Heckman et al. 1990; Meurer et al. 1995; Lehnert & Heckman 1996) and distant starbursting galaxies including ULIRGs (Sanders & Mirabel 1996) and LBGs (e.g., Adelberger & Steidel 2000). Note that $\kappa > \kappa_{\text{crit}}$ can be obtained even for very subsolar metallicities ($\lesssim 0.1$ solar), suggesting that the momentum-driven outflows considered here may be important even for the formation of relatively “primordial” galaxies.

It is worth considering how and in what quantity dust is created in young galaxies. Dust can be created in AGB stars, but the timescale to do so is ~ 1 Gyr, long compared to the duration of a starburst, and so may not dominate the production of dust in young galaxies. Instead, Kozasa et al. (1989), Todini & Ferrara (2001), and Nozawa et al. (2003) show that SNe can produce $M_{\text{dust}} \sim 0.5 M_{\odot}$ of dust per SN, depending on the progenitor metallicity and mass. To an order of magnitude, where \mathcal{L} is the scale of the system, the number of SNe required to yield $\tau_{\text{dust}} \sim 1$ in the volume $(4\pi/3)\mathcal{L}^3$ is

$$N_{\text{SN}} \sim 10^6 \left(\frac{\mathcal{L}}{2 \text{ kpc}} \right)^2 \left(\frac{0.5 M_{\odot}}{M_{\text{dust}}} \right) \left(\frac{10^4 \text{ cm}^2 \text{ g}^{-1}}{\kappa_{\text{dust}}} \right), \quad (30)$$

where κ_{dust} is the opacity in units of $\text{cm}^2 \text{ g}^{-1}$ of *dust* (note that throughout the rest of this paper κ is expressed in units of $\text{cm}^2 \text{ g}^{-1}$ of *gas*; we use κ_{dust} in eq. [30] because the result can then be expressed independent of the gas mass or gas-to-dust ratio). For an SN rate of 10^{-2} yr^{-1} for every solar mass per year of star formation, the timescale for SNe to generate $\tau_{\text{dust}} \sim 1$ is $\sim 10^8 \dot{M}_{*}^{-1} \text{ yr}$. This timescale is reasonably short and so we expect that the required opacity may be produced either by quiescent star formation or during a starburst itself. For example, in a large starburst with $\dot{M}_{*} \sim 100 M_{\odot} \text{ yr}^{-1}$, $\tau_{\text{dust}} \sim 1$ is reached in just $\sim 10^6 \text{ yr}$ (or soon after the first SNe occur).

2.6. The Coupling between Dust and Gas

The mean free path for scattering of dust and gas is simply $\lambda = (n\sigma_{\text{dg}})^{-1}$, where n is the gas number density and σ_{dg} is the dust-gas scattering cross section. Since we require that order unity of the dust momentum be imparted to the gas, the quantity of interest is $\lambda_M = \lambda(m_D/m_p)$, where m_D is the mass of an individual dust grain. For a grain of radius a and a geometric cross section, we estimate

$$\lambda_M \simeq 10 a_{0.1} \rho_3 n_1^{-1} \text{ pc}, \quad (31)$$

where $a_{0.1} = a/(0.1 \mu\text{m})$, n_1 is the number density of gas, normalized to one particle per cm^3 , and ρ_3 is the mass density of an individual dust grain, normalized to 3 g cm^{-3} . To assess the hydrodynamical coupling of dust and gas, we compare λ_M with the radial scale R in the galaxy. We leave to future work a detailed multifluid model of dust-driven galactic winds (as in models of winds from cool stars).

In a sufficiently low density phase of the ISM, it is possible to have $\lambda_M > R$ and thus for dust and gas to be hydrodynamically decoupled. In this case dust could be expelled from a galaxy without the gas (e.g., Davies et al. 1998). It seems, however, more likely that the dust is present in the cold, dense phase of the ISM with $n_1 \gtrsim 1$, in which case $\lambda_M \ll R$ and the dust

efficiently shares the radiative momentum it receives with the gas. As the flow moves outward, however, the density of gas decreases and λ_M may eventually exceed the radius R . To estimate the radial scale at which this happens (R_{dg}), we use $n = \dot{M}_W/(4\pi m_p R^2 V)$ to estimate the gas density (with \dot{M}_W from eq. [20] and $V \sim \sigma$). Combining with equation (31), we find that $\lambda_M > R$ at

$$R_{\text{dg}} = \frac{3}{4\pi} \frac{\sigma^2 f_g}{\rho_D a G} \sim 150 \rho_3^{-1} a_{0.1}^{-1} \sigma_{200}^2 f_{g_{0.1}} \text{ kpc}. \quad (32)$$

Because R_{dg} is significantly larger than the scale on which the outflow is accelerated, we expect the dust and gas to be well coupled in the acceleration region and thus that the gas can be blown out of the galaxy with the dust. This estimate of R_{dg} is probably conservative because the dust may primarily be in cold gas clouds whose density will not decrease as R^{-2} as for the continuous wind considered above. Note also that near the source of UV photons the dust grains will be charged. This will further increase the coupling of the dust to the gas, both because of Coulomb collisions (Draine & Salpeter 1979) and because the Larmor radius of the dust will be sufficiently small that the dust is magnetically coupled to the gas.

3. ENERGY-DRIVEN GALACTIC WINDS

Several properties of winds generated by energy deposition are different from those driven by momentum deposition. To highlight the differences, we briefly review the physics of the former in the galactic context (for analytic solutions see, e.g., Chevalier & Clegg 1985).

Given a total energy deposition rate \dot{E} (ergs s^{-1}), one may estimate the mass-loss rate of an energy deposition-driven wind by equating the asymptotic kinetic energy loss rate with \dot{E} ,

$$\frac{1}{2} \dot{M}_W V_{\infty}^2 \approx \dot{E}. \quad (33)$$

For a starburst galaxy the energy injection is provided by SNe and winds from massive stars, with comparable energy from each source (Leitherer et al. 1999). We focus on SNe here. Assuming that each SN yields an energy of $\sim 10^{51}$ ergs, the total energy deposition rate from SNe is

$$\begin{aligned} \dot{E}_{\text{SN}} &= \xi E_{\text{SN}} \Gamma_{\text{SN}} \sim \xi E_{\text{SN}} \dot{M}_{*} f_{\text{SN}} \\ &\sim 3 \times 10^{40} \xi_{0.1} \left(\frac{\dot{M}_{*}}{1 M_{\odot} \text{ yr}^{-1}} \right) \text{ ergs s}^{-1}, \end{aligned} \quad (34)$$

where ξ is the efficiency of energy transfer to the ISM ($\xi_{0.1} = \xi/0.1$ implies 10% efficiency), Γ_{SN} is the number of SNe per unit time, and $f_{\text{SN}} \approx 10^{-2}$ is the number of SNe per solar mass of star formation. The efficiency ξ with which SN energy is transferred to the ISM is uncertain and depends on, e.g., the density of the ISM. Thornton et al. (1998) showed that SN remnants typically radiate at least 90% of their energy during their evolution. Hence, only $\sim 10\%$ may be efficiently thermalized in the ISM. We normalize ξ to this value but emphasize that it is uncertain.

Comparing equation (34) with equation (11), we see that, absent radiative losses ($\xi = 1$), \dot{E}_{SN} can be written simply in terms of the starburst luminosity as $\dot{E}_{\text{SN}} \sim 10^{-2} L_{\text{SB}}$. The factor of 100 appearing in this relationship comes from the fact that a typical massive star releases $\sim 10^{53}$ ergs in luminous energy over its lifetime, whereas it deposits $\sim 10^{51}$ ergs during its SN (e.g., Abbott 1982).

Equations (33) and (34) can be combined to give an expression for the mass-loss rate in energy-driven winds,

$$\dot{M}_W \approx \dot{M}_* \left(\frac{\xi \epsilon 10^{-2} c^2}{V_\infty^2} \right) \approx \dot{M}_* \xi_{0.1} \epsilon_3 \left(\frac{300 \text{ km s}^{-1}}{V_\infty} \right)^2. \quad (35)$$

For fiducial numbers this estimate is similar to our estimate of the mass-loss rate in momentum-driven winds (eq. [13]). However, equations (35) and (13) differ in two important ways. First, if the SN energy is efficiently radiated away ($\xi \ll 1$), equation (35) predicts a mass-loss rate much less than equation (13). Second, momentum-driven winds yield the scaling $\dot{M}_W \propto \dot{M}_*/V_\infty$, whereas energy-driven winds predict $\dot{M}_W \propto \dot{M}_*/V_\infty^2$. This difference in scaling may be observationally testable.

We estimate the energy injection required to unbind the gas in a galaxy by requiring that $\dot{E}_{\text{SN}} \tau_{\text{dyn}} \gtrsim E_{\text{bind}}$, where $E_{\text{bind}} = GMM_g/r$ and $\tau_{\text{dyn}} \sim r/\sigma$. This yields $\dot{E}_{\text{SN}} \gtrsim 4f_g \sigma^5/G$. Rewriting this in terms of the corresponding starburst luminosity gives

$$L_E \sim \frac{100}{\xi} \frac{4f_g}{G} \sigma^5 \sim 2 \times 10^{46} f_{g,0.1} \xi_{0.1}^{-1} \sigma_{200}^5 \text{ ergs s}^{-1}, \quad (36)$$

where the subscript “ E ” stands for “energy-driven,” in contrast to L_M (eq. [15]). Equation (36) is a criterion to “blow away” all of the gas of the galaxy (following the nomenclature of De Young & Heckman 1994). In a disk galaxy, SNe may “blow out” in the direction perpendicular to the disk (even for L_{SB} less than L_E), but in this case very little of the gas mass of the galaxy will be affected (e.g., De Young & Heckman 1994). In fact, the numerical simulations of Mac Low & Ferrara (1999) and Strickland & Stevens (2000) find that SN energy thermalized in the ISM can be efficiently vented when the remnants break out of the galactic disk. However, very little of the mass in the galaxy is actually blown away.

3.1. Entrainment

A hot wind can in principle sweep up and entrain embedded clouds of cold gas, driving them out of the galaxy by ram pressure. The cold gas may also be shock heated and evaporated by the hot flow. The energy-driven limit considered in the previous subsection is appropriate when most of the cold gas is shock heated and incorporated into the hot flow (and radiative losses are small). In the opposite limit, in which the cold gas retains its identity, the dynamics of the cold gas is analogous to that of a momentum-driven wind because it is pushed out by the ram pressure of the hot gas. In the Appendix we show this explicitly by demonstrating that the ram pressure and radiation pressure forces on cold clouds are typically comparable (eq. [A1]). We also derive both the optically thin (eq. [28]) and optically thick (eq. [15]) Eddington luminosities discussed in § 2.2 using ram pressure as the acceleration mechanism (rather than radiation pressure); see, in particular, equations (A4) and (A7).

Distinguishing which of these two mechanisms actually dominates the acceleration of cold gas is an important but difficult problem. It is, in particular, unclear whether embedded clouds can actually survive entrainment in a hot flow. Calculations show that the clouds are typically destroyed in a few cloud crossing times (e.g., Klein et al. 1994; Poludnenko et al. 2002), although considerable cloud material can be accelerated to high velocity in the process. In the Appendix we focus on the

acceleration of cloud material to highlight the analogy between ram pressure and radiation pressure driving of cold gas, but the acceleration, ablation, and destruction of the clouds likely go hand in hand.

3.2. Comparing Momentum-driven and Energy-driven Winds

Equation (36) defines the starburst luminosity above which energy injection by SNe is sufficient to unbind all of the gas in the galaxy. Comparing this limiting luminosity with the corresponding expression for momentum-driven winds (L_M ; eq. [15]), we see that $L_M \sim L_E$ at a critical velocity dispersion

$$\sigma_{\text{crit}} = \frac{\xi}{100} c \sim 300 \xi_{0.1} \text{ km s}^{-1}. \quad (37)$$

For $\sigma < \sigma_{\text{crit}}$, $L_E < L_M$ and one might expect energy deposition via SNe to dominate feedback on the ISM. By contrast, for $\sigma > \sigma_{\text{crit}}$, $L_M < L_E$ and momentum deposition dominates and is sufficient to blow all of the gas out of the galaxy (this is true regardless of whether the primary source of momentum deposition is radiation pressure or SNe). Note that because of the many simplifications made in deriving L_M and L_E , the actual value for σ_{crit} is only accurate to an order of magnitude; it is also very sensitive to assumptions about the efficiency with which SN energy is thermalized in the ISM. In § 4 we show that dwarf starbursting galaxies violate equation (36) by several orders of magnitude. This suggests that in practice σ_{crit} is quite small, significantly smaller than the nominal value in equation (37).

The scale σ_{crit} sets a lower bound on the range of σ over which the luminosity limit L_M is applicable. There is also an upper bound. In equations (22) and (23) we estimated (very crudely) the maximum star formation rate and luminosity attainable in a starburst and the σ_{max} above which a system cannot generate a luminosity $\sim L_M$.

Figure 1 illustrates these bounds and the limiting luminosities schematically. The two limiting luminosities ($L_E \propto \sigma^5$ and $L_M \propto \sigma^4$), as well as the maximum attainable luminosity ($L_{\text{max}} \propto \sigma^3$; eq. [22]), are sketched as a function of σ . The limit L_M is applicable in the region $\sigma_{\text{crit}} < \sigma < \sigma_{\text{max}}$. For reference, the FJ relation for elliptical galaxies and bulges is also sketched. It has a lower “zero point” than L_M , but the same dependence on σ , $L_{\text{FJ}} \propto \sigma^4$. We discuss this correlation and its relation to L_M in detail in the next section, but note here that deviations from the FJ relation are possible for $\sigma < \sigma_{\text{crit}}$ and $\sigma > \sigma_{\text{max}}$.

4. STARBURST GALAXIES AND THE FABER-JACKSON RELATION

In this section we apply the idea of “Eddington-limited” star formation to star-forming galaxies at high redshift. The basic scenario is as follows. The luminosity of a nuclear starburst increases as it forms stars. When the luminosity increases to L_M (eq. [15]), the starburst drives gas out of the galactic potential and regulates its luminosity to $\approx L_M$ (a similar idea has been proposed by Elmegreen 1983 and Scoville et al. 2001 for what determines the mass and luminosity of individual star clusters; Scoville 2003 discussed a limit directly analogous to our optically thin limit L_{Edd} , eq. [25]). We argue that this self-regulation determines the total number of stars formed in a given dark matter potential well. First, we describe observations showing that star formation rates sufficient to produce $L \approx L_M$ do occur in star-forming galaxies at both high and low redshifts. Then we show that if all early-type galaxies went through such a star

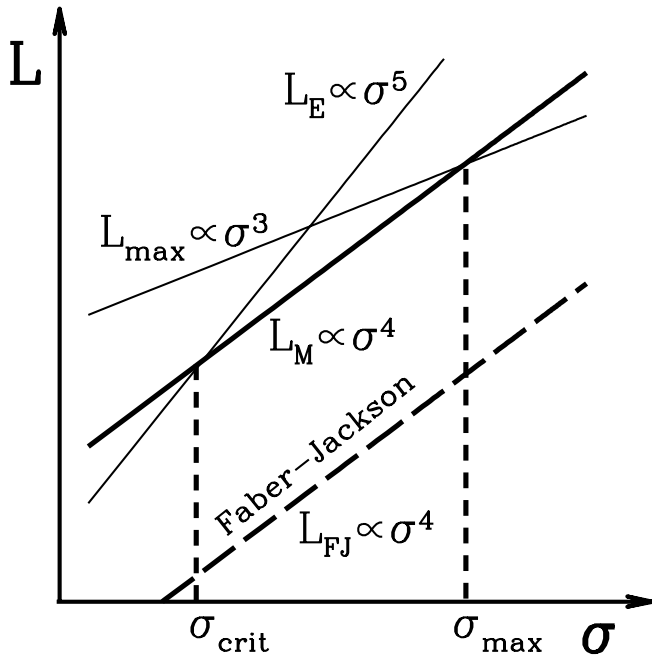


FIG. 1.—Schematic diagram of the limiting starburst luminosity for momentum-driven galactic winds as a function of σ ($L_M \propto \sigma^4$; eq. [15]; *thick solid line*). The thin solid lines show the maximum attainable starburst luminosity determined by converting all of the available gas into stars on a dynamical time ($L_{\max} \propto \sigma^3$; eq. [22]) and the limiting starburst luminosity for energy-driven galactic winds ($L_E \propto \sigma^5$; eq. [15]). For $\sigma < \sigma_{\text{crit}}$ (eq. [37]), energy-driven winds dominate wind driving and feedback because $L_E < L_M$. The value of σ_{crit} depends sensitively on the fraction of the kinetic energy injected by an SN that is radiated away (§ 3.2). Because the starburst luminosity is bounded by L_{\max} , for $\sigma > \sigma_{\max}$ (eq. [23]), the starburst cannot reach L_M . In the intermediate region where $\sigma_{\text{crit}} < \sigma < \sigma_{\max}$, the starburst luminosity is bounded by L_M and momentum deposition dominates wind driving and feedback. As we argue in § 4, this effect sets the FJ relation for elliptical galaxies. The FJ relation, $L_{\text{FJ}} \propto \sigma^4$, is sketched here for comparison with the other luminosity limits (*thick dashed line*). It has a lower zero point than L_M as a result of passive, poststarburst evolution of the stellar population. This schematic plot is to be compared with Fig. 2, which shows the observed FJ relation and data from local and high-redshift starburst galaxies. Fig. 2 suggests that the limit L_M , rather than L_E , is relevant down to quite small $\sigma \sim 20 \text{ km s}^{-1}$.

formation episode at $z \gtrsim 1$, self-regulation at $\approx L_M$ can explain the FJ relation.

4.1. The Maximum Luminosity $L_M(\sigma)$: Observations

Figure 2 shows the luminosity as a function of the velocity dispersion for a sample of high star formation rate galaxies drawn from the literature. We also plot the expression for L_M (eq. [15]) for three values of the gas fraction $f_g = 1, 0.1, \text{ and } 0.01$. These different curves should be taken to include both plausible variations in the gas fraction (which changes in time) and uncertainty in the value of L_M . The latter arises because the total momentum deposition rate may be somewhat larger than just L/c since contributions from SNe, stellar winds, and starburst photons are all comparable. In addition, photons may be absorbed several times as they exit the starburst region and the galaxy.

In collecting the data in Figure 2, we attempted to find representative examples of the highest star formation rate galaxies at a variety of σ (see Tables 1 and 2 for details). This includes dwarf galaxies (Mateo 1998; Martin 1998), LBGs at $z \approx 2$ (Erb et al. 2003) and $z \approx 3$ (Pettini et al. 2001), ULIRGs locally (Genzel et al. 2001) and at high redshift (Neri et al. 2003; Genzel et al. 2003; Tecza et al. 2004), galaxies from the

Canada-France Redshift Survey (CFRS) at $z \approx 0.6$ (Lilly et al. 1996; Mallén-Ornelas et al. 1999), and a sample of local starbursts (Heckman et al. 2000). For the local starbursts we chose a sample of systems that clearly show evidence for outflowing *cold* gas. Even though many systems fall significantly below the L_M curve, radiation pressure is sufficient to generate an outflow of cold gas comparable to what is observed because the radiation pressure force on individual gas clouds can exceed gravity even if $L \ll L_M$ (since the latter criterion refers to blowing out *all* of the gas in the galaxy). We will discuss this in more detail in a future paper.

The data in Figure 2 are necessarily heterogeneous, and there are uncertainties in both luminosities and velocity dispersions, but this compilation illustrates several important points. First, the simple momentum driving limit given by equation (15) does provide a reasonable upper limit to the luminosity of observed starbursting systems. The fact that some systems fall below this limit is, of course, no surprise. They might simply not have star formation rates sufficient to reach L_M , or they might be observed somewhat after the peak star formation episode (which is, after all, where systems spend most of their time; see Fig. 3).

It is also worth stressing that the upper envelope to the observed luminosity as a function of σ is incompatible with the simple limit based on energy feedback from SNe, which predicts $L_E \propto \sigma^5$ (§ 3; eq. [36]). In particular, the low- σ systems in Figure 2 have luminosities well in excess of the energy limit given in equation (36). This implies that either the efficiency of transferring SN energy to the ISM is very low (e.g., $\xi \sim 10^{-2}$) or else SNe do not globally halt star formation by ejecting most of the gas (e.g., because the SNe blow out of the galactic plane; De Young & Heckman 1994). In either interpretation, this argues for $\sigma_{\text{crit}} \lesssim 20 \text{ km s}^{-1}$ (see Fig. 1), in which case momentum injection may dominate the global mass loss in many starbursting systems.

For the purposes of this paper, perhaps the most interesting feature of Figure 2 is that starbursting galaxies at high redshift have luminosities reasonably close to L_M . This includes both LBGs, ULIRGs, and galaxies drawn from the CFRS of Lilly et al. (1996). We suggest that this is not a coincidence but is instead evidence that star formation at high redshifts self-regulates; when the starburst reaches a luminosity $\sim L_M$, the galaxy drives a powerful wind that limits the available gas supply and thus the star formation rate. This feedback mechanism regulates the luminosity of the starburst and ultimately helps set the stellar mass of the galaxy.

The $z \gtrsim 1$ galaxies shown in Figure 2 are representative of systems that have been used to study the star formation history of the universe (e.g., Madau et al. 1996; Steidel et al. 1999). It is known that integrating the inferred star formation history over redshift can account reasonably well for the total stellar mass density observed at $z = 0$ (Madau et al. 1998).

The fact that many of the individual systems that comprise the “Madau” plot have $L \sim L_M$ thus suggests that a significant fraction of the stellar mass in the universe has been built up through starbursts that self-regulate by momentum-driven galactic winds. We show in the next section that if this hypothesis is correct, it can account for the FJ relation.

A direct test of our hypothesis is that rapidly star-forming galaxies at high redshift should drive powerful galactic winds. Powerful winds are seen in LBGs (e.g., Pettini et al. 2000; Adelberger et al. 2003). It is, however, difficult to isolate the physical mechanism responsible for driving such outflows. One prediction of the momentum-driven wind model is that observed

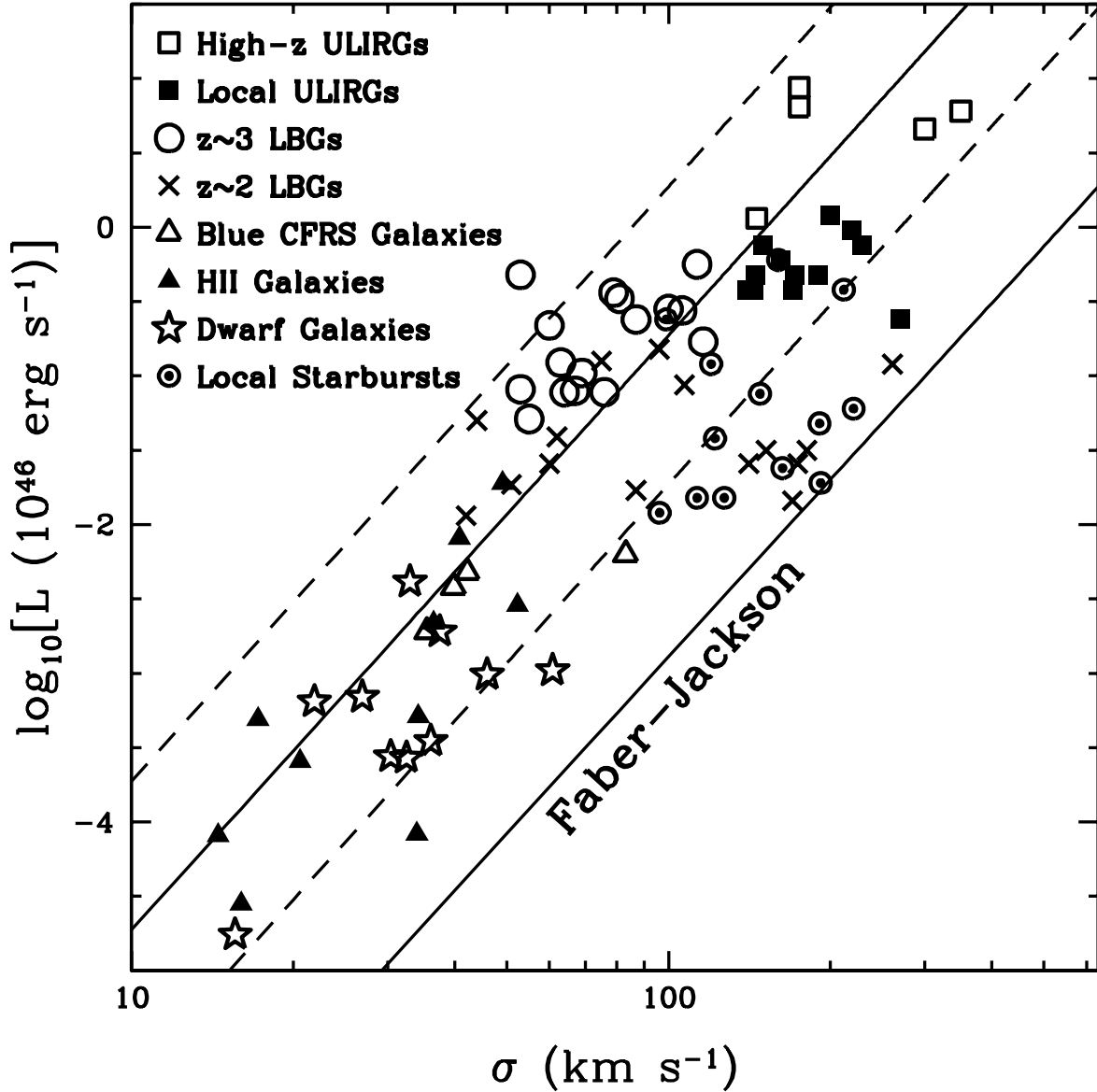


FIG. 2.—Limiting luminosity for momentum-driven galactic winds (L_M ; eq. [15]) as a function of the velocity dispersion σ , for three values of the gas fraction ($f_g = 0.1$, thick solid line; $f_g = 1.0$ and 0.01 , dashed lines). These curves also account for uncertainty associated with the net momentum deposition rate in starbursts, which includes contributions from radiation, stellar winds, and SNe. Also shown is the observed FJ relation from eq. (38). From §§ 2.2 and 4, we predict that for $\sigma_{\text{crit}} < \sigma < \sigma_{\text{max}}$ (see Fig. 1), no system should have a luminosity greater than L_M . We test this prediction in this figure by surveying the literature for the brightest objects at any σ . Detailed information on all systems plotted here can be found in Tables 1 and 2 and the references cited therein. The open squares show high-redshift ULIRGs ($z \sim 2-3$), taken from Genzel et al. (2003), Neri et al. (2003), and Tecza et al. (2004). The filled squares show local ULIRGs (Genzel et al. 2001, their Tables 1 and 2). The $z \sim 3$ LBGs are shown by open circles (Pettini et al. 2001), while the $z \sim 2$ LBGs are shown by crosses (Erb et al. 2003). The open triangles are taken from the sample of blue CFRS galaxies at $z \sim 0.6$ in Mallén-Ornelas et al. (1999, their Fig. 2). We have selected the brightest galaxies at several σ . The filled triangles show the sample of H II galaxies from Telles & Terlevich (1997, their Tables 1 and 3). The open stars are dwarf galaxies from Martin (1998) and Mateo (1998, Tables 4 and 7). The subset of dwarfs plotted here are those with the highest luminosities associated with current star formation, rather than the old stellar population. Finally, we include a selection of local starbursts from Heckman et al. (2000) that show evidence for outflows of cold gas (see Table 2 for details). [See the electronic edition of the Journal for a color version of this figure.]

outflows should have a momentum flux $\dot{M}_W V_\infty$ comparable to that of the starburst, L/c . This can be rewritten as (eq. [13]) $\dot{M}_W \approx \dot{M}_*(c\epsilon/V_\infty)$. This prediction is difficult to test because it is hard to reliably measure the mass outflow rate \dot{M}_W .

The best case so far at high redshift is probably the gravitationally lensed LBG MS 1512-cB58. Pettini et al. (2000) estimate a mass-loss rate of $\approx 60 M_\odot \text{ yr}^{-1}$ and an outflow velocity of $V_\infty \approx 200 \text{ km s}^{-1}$. The inferred star formation rate is $\dot{M}_* \approx 40 M_\odot \text{ yr}^{-1}$, suggesting a close correspondence between the momentum input from stars and that in the outflow.

4.2. The Faber-Jackson Relation

The FJ relation connects the luminosity of the bulge or spheroidal component of a galaxy with its velocity dispersion (Faber & Jackson 1976; for a review see Burstein et al. 1997). Bernardi et al. (2003, their Fig. 4) give the FJ relation derived from about 9000 early-type galaxies in the Sloan Digital Sky Survey (SDSS). In the i band, their results imply

$$\nu L_{\nu,i} \simeq 2 \times 10^{44} \sigma_{200}^{3.95} \text{ ergs s}^{-1} \quad (38)$$

TABLE 1
LUMINOSITY AND VELOCITY DISPERSION: HIGH-REDSHIFT GALAXIES

Object Class	Name	$\log_{10}L$ (L_{\odot})	σ (km s^{-1})	References	Notes
High- z ULIRGs.....	SMM J14011+0252	13.36	175	1	1
	SMM J02399-0136	13.08	300	2	
	SMM J04431+0210	12.48	146	3	
	SMM J09431+4700	13.23	175	3	
	SMM J16368+4057	13.20	350	3	
$z \sim 3$ LBGs.....	CDFa D18	11.98	79	4	2
	CDFa C8	11.86	106	4	
	CDFa C1	11.51	≤ 63	4	
	Q0201+113 C6	11.31	64	4	
	Q0256-000 C17	11.33	53	4	
	Q0347-383 C5	11.44	69	4	
	B2 0902+343 C12	11.80	87	4	
	West MMD11	12.10	53	4	
	Q1422+231 D81	11.65	116	4	
	3C 324 C3	11.31	76	4	
	SSA 22a MD46	11.32	67	4	
	SSA 22a D3	12.17	113	4	
	DSF 2237+116a C2	11.87	100	4	
	B2 0902+343 C6	12.13	55	4	
	MS 1512-cB58	11.94	81	4	
	Q0000-263 D6	11.76	60	4	
$z \sim 2$ LBGs.....	CDFb-BN88	11.60	96	5	3
	Q0201-B13	11.01	62	5	
	Westphal BX600	10.92	181	5	
	Q1623-BX376	11.50	261(a), <224(b)	5	
	Q1623-BX432	10.69	51	5	
	Q1623-BX447	10.83	174	5	
	Q1623-BX449	10.83	141	5	
	Q1623-BX511	10.92	152	5	
	Q1623-BX522	11.12	<44	5	
	Q1623-MD107	10.48	<42	5	
	Q1700-BX691	10.58	170	5	
	Q1700-BX717	10.83	<60	5	
	Q1700-MD103	11.52	75	5	
	Q1700-MD109	10.65	87	5	
SSA22a-MD41	11.36	107	5		
$z \sim 0.6$ CFRS	CFRS-1	9.70	35	6	4
	CFRS-2	10.00	40	6	
	CFRS-3	10.10	42	6	
	CFRS-4	10.22	83	6	

NOTES.—(1) For object SMM J14011+0252, the luminosity was determined using $L = L_{\text{IR}}$ and the velocity dispersion was determined by using $\sigma = V_{\text{circ}}/\sqrt{2}$. For the remaining four systems, the luminosity was determined using $L = L_{\text{IR}}$ and the velocity dispersion was determined by using $\sigma = \text{LW}/2.4$, where LW is the line width. (2) For all systems, L was obtained from AB magnitude: $L = \nu L_{\nu} 10^{-0.4M_{\text{UV}}}$, where $L_{\nu} = 4.3 \times 10^{20} \text{ ergs s}^{-1} \text{ Hz}^{-1}$. Bolometric luminosities for all systems are extinction corrected. The extinction, $E(B - V)$, was computed from the $(G - R)$ color (A. Shapley 2004, private communication). The velocity dispersion quoted for all systems (σ) is the one-dimensional velocity dispersion of nebular lines. (3) For all systems, L was obtained from the extinction-corrected UV SFR: $\text{SFR} = 1.4 \times 10^{-28} L_{1500} \text{ ergs s}^{-1} \text{ Hz}^{-1}$. For all systems, the velocity dispersion is as quoted in Table 2 of Erb et al. (2003). For system Q1623-BX376 we use $\sigma = 261 \text{ km s}^{-1}$ in Fig. 2. For systems Q1623-BX522, Q1623-MD107, and Q1700-BX717 we plot the upper bound on σ in Fig. 2. (4) For all systems, L is obtained from M_B with $h = 0.7$: $L = 4.73 L_{B,\odot} 10^{-0.4(M_B - 5.48)}$.

REFERENCES.—(1) Tecza et al. 2004; (2) Genzel et al. 2003; (3) Neri et al. 2003; (4) Pettini et al. 2001; (5) Erb et al. 2003; (6) Mallén-Ornelas et al. 1999.

over the range $\sigma \approx 100\text{--}300 \text{ km s}^{-1}$. The slope of the FJ relation is nearly identical in all of the SDSS bands, while the normalization decreases slightly (by a factor of ≈ 2) at the shortest wavelengths (the g band). In a separate analysis Pahre et al. (1998) give the FJ relation in the near-infrared (K band), finding $\nu L_{\nu,K} \simeq (3 \times 10^{43} \text{ ergs s}^{-1}) \sigma_{200}^{4.1}$. Thus, the slope of the FJ relation is essentially independent of wavelength while the change in its normalization with wavelength is consistent with the spectrum of an old stellar population. That is, if one plots

the normalization of the FJ relation as a function of wavelength, the resulting ‘‘spectrum’’ is very similar to that produced by a ~ 10 Gyr old instantaneous starburst.¹⁰

¹⁰ Such an exercise is only possible because the slope of the FJ relation is independent of σ so one can meaningfully construct a spectrum. In particular, it is not possible to carry out the same procedure for disk galaxies because the slope of the Tully-Fisher relation increases with increasing wavelength (Binney & Merrifield 1998).

TABLE 2
LUMINOSITY AND VELOCITY DISPERSION: LOW-REDSHIFT GALAXIES

Object Class	Name	$\log_{10}L$ (L_{\odot})	σ (km s^{-1})	References	Notes
Local ULIRGs	I00262+4251	12.0	170	1	1
	I00456–2901	12.2	162	1	
	I01388–4618	12.0	144	1	
	I01572+0009 Mrk 1014	12.5	200	1	
	I14348–1447	12.3	150(u), 170(l)	1	
	I15327+2340 Arp 220	12.1	172(W), 155(E)	1	
	I16504+0228 NGC 6240	11.8	270(N), 290(S)	1	
	I17208–0014	12.3	229	1	
	I20087–0308	12.4	219	1	
	I20551–4250	12.0	140	1	
	I23365+3604	12.1	145	1	
	I23578–5307	12.1	190	1	
	H II galaxies	UM 133	9.11	17.2	2, 3
C0840+1044		8.34	34.0	2, 3	
C0840+1201		9.76	36.5	2, 3	
C08-28A		10.70	49.1	2, 3	
Mrk 36		7.87	16.0	2, 3	
UM 448		10.33	40.8	2, 3	
UM 455		8.83	20.6	2, 3	
UM 461A		8.33	14.5	2, 3	
C1212+1148		9.13	34.2	2, 3	
C1409+1200		9.88	52.3	2, 3	
Dwarf galaxies	WLM	7.66	15.6	4	3
	NGC 55	9.44	60.8	4	
	NGC 6822	8.96	36.1	4	
	IC 10	10.03	33.0	4	
	II Zw 40	9.18	35.2	5	
	NGC 1569	9.23	21.9	5	
	NGC 4861	8.86	30.4	5	
	NGC 1800	8.85	32.5	5	
	NGC 3077	9.41	45.96	5	
	NGC 5253	9.26	26.9–42.4	5	
	Local starbursts	IRAS 03514+1546	11.1	191	6
NGC 1572		11.2	221	6	
NGC 1614		11.3	148	6	
IRAS 04370–2416		11.0	122	6	
NGC 1808		10.6	113	6	
NGC 2146		10.7	192	6	
M82		10.5	96.2	6	
IRAS 10173+0828		11.8	99	6	
NGC 3256		11.5	120	6	
IRAS 10565+2448		12.0	212	6	
Mrk 273		12.2	160	6	
NGC 7582		10.6	127	6	
NGC 7552		10.8	163	6	

NOTES.—(1) The luminosity and velocity dispersion for all systems are taken from Tables 1 and 2 of Genzel et al. (2001). In cases in which two σ -values are observed, we plot the lower of the two in Fig. 2. This applies to I14348–1447, Arp 220, and NGC 6240. (2) For all systems, L is obtained from M_V (Table 3 of Telles & Terlevich 1997) via $L = 6.3L_{V,\odot}10^{-0.4(M_V - 4.83)}$. These luminosities are corrected for galactic extinction only. For all systems σ is the rms velocity dispersion from Table 1 of Telles & Terlevich (1997). (3) For WLM, NGC 55, NGC 6822, and IC 10, the luminosity was determined directly from the SFR by $L = \epsilon M_* c^2$ with $\epsilon = 10^{-3}$. For these systems, the velocity dispersion was obtained from the circular velocity: $\sigma = V_{\text{circ}}/(\sqrt{2} \sin i)$. For II Zw 40, NGC 1569, NGC 4861, NGC 1800, NGC 3077, and NGC 5253, the luminosity was determined directly from the SFR by $L = \epsilon M_* c^2$ with $\epsilon = 10^{-3}$. For these systems, the velocity dispersion was obtained from the circular velocity: $\sigma = V_{\text{circ}}/\sqrt{2}$. For NGC 5253, we plot $\sigma = 26.9 \text{ km s}^{-1}$. (4) The luminosity for each system is from Heckman et al. (2000). The velocity dispersion for every system except M82 and Mrk 273 is also taken from Heckman et al. (2000). For M82, σ is taken from Martin (1998). For Mrk 273, σ is taken from Genzel et al. (2001). For each system, the velocity dispersion is determined from the rotational velocity by $\sigma = V_{\text{rot}}/\sqrt{2}$.

REFERENCES.—(1) Genzel et al. 2001; (2) Telles & Terlevich 1997; (3) Melnick et al. 1988; (4) Mateo 1998; (5) Martin 1998; (6) Heckman et al. 2000.

Our expression for the limiting starburst luminosity is given in equations (15) and (18). This luminosity corresponds to that *during* the starburst, whereas equation (38) is a statement about L and σ *now*. If, as we have argued above, most (all) early-type galaxies went through a significant starburst phase during

which their luminosities reached, but did not exceed, our limiting luminosity, we can determine the properties of the stellar population now by “fading” the starburst with time.

Figure 3 shows the luminosity of a starburst as a function of time in the models of Bruzual & Charlot (2003). Starbursts of

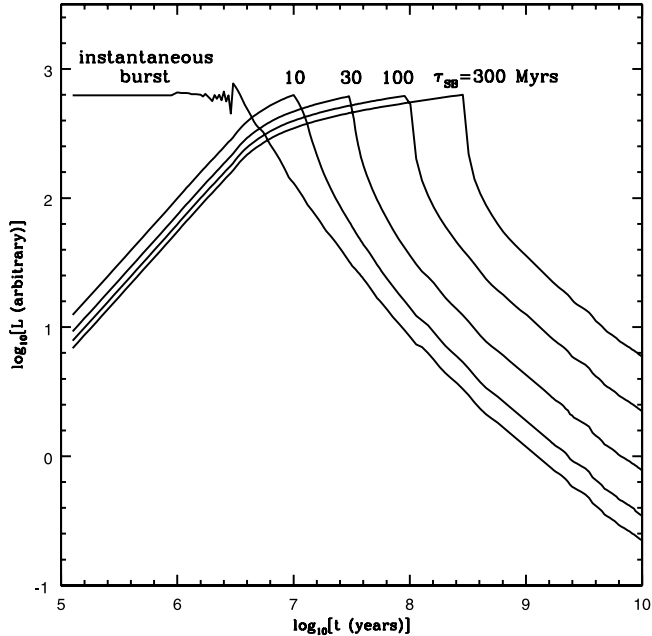


FIG. 3.—Starburst luminosity as a function of time in the models of Bruzual & Charlot (2003), for an instantaneous starburst and starbursts with duration $\tau_{\text{SB}} = 10, 30, 100,$ and 300 Myr. All calculations were normalized to the same peak luminosity and employ a Salpeter IMF from 0.1 to $100 M_{\odot}$. We argue that the ratio between the peak starburst luminosity and the luminosity at 10^{10} yr gives the normalization between L_M (eqs. [15] and [18]) and the present-day FJ relation (eq. [38]). This requires a starburst lifetime of $\tau_{\text{SB}} \sim 300$ Myr.

five durations are shown: instantaneous, 10 Myr, 30 Myr, 100 Myr, and 300 Myr (with constant star formation rates and a Salpeter IMF between 0.1 and $100 M_{\odot}$). The ratio of the peak starburst luminosity to the luminosity now ($t \sim 10^{10}$ yr) determines how much the stellar population fades with time and allows us to connect the maximum starburst luminosity to the currently observed FJ relation. For the models shown in Figure 3 the starburst fades by a factor of 2500, 1500, 800, 250, and 100 over $\approx 10^{10}$ yr. These results can be understood analytically by noting that, for a Salpeter IMF and a stellar mass-luminosity relation of the form $L \propto M^{\beta}$, the late-time luminosity of a starburst is given by

$$L(t) \sim 3L_{\text{SB}} \left(\frac{\tau_{\text{SB}}}{\tau_{\text{max}}} \right) \left(\frac{t}{\tau_{\text{max}}} \right)^{-(\beta-1.35)/(\beta-1)}, \quad (39)$$

where $\tau_{\text{max}} \approx 3$ Myr is the lifetime of the most massive stars, τ_{SB} (assumed $> \tau_{\text{max}}$) is the duration of the starburst, and L_{SB} is the peak luminosity of the starburst; the factor of 3 has been included based on comparison to numerical calculations. The dependence on $\tau_{\text{SB}}/\tau_{\text{max}}$ seen in Figure 3 and equation (39) arises because the late-time luminosity is determined by the total number of low-mass stars made during the burst, while the peak starburst luminosity (L_{SB}) depends only on the instantaneous number of massive stars present in the starburst. For $\beta \approx 4-5$, equation (39) predicts $L(t) \propto t^{-0.9}$, in reasonable agreement with Figure 3 at late times.

Comparing the observed FJ relation with the maximum starburst luminosity in equation (15) shows that if the starburst fades by a factor of $\approx 100-200$ from $z \sim \text{few}$ to now, then we can account for both the normalization and slope of the FJ relation as being due to feedback during the formation of elliptical galaxies at high redshift. This in turn requires that most of the stars in a galaxy were formed over a period of $\tau_{\text{SB}} \sim$

$100-300$ Myr (Fig. 3).¹¹ This number is plausible on a number of grounds. It is comparable to the inferred star formation timescales in LBGs (e.g., Shapley et al. 2001) and ULIRGs (e.g., Genzel et al. 2004). It is also comparable to the dynamical timescale τ_{dyn}^D of gas on galactic scales. This is relevant because this dynamical timescale roughly determines the duration of starbursts in numerical simulations of merging galaxies (Mihos & Hernquist 1996).

The scatter in the FJ relation is observed to be a factor of ≈ 2 in L at a given σ (Bernardi et al. 2003). In our model, this scatter is primarily due to differences in the time since, and duration of, the star formation episode that built up most of the mass of the galaxy. Since most early-type galaxies likely formed at $z \sim 1-3$ and the time difference between these redshifts is only a factor of ≈ 1.5 , the scatter produced in the observed FJ by different “formation redshifts” is quite mild (since $L \sim t^{-1}$; see Fig. 3). By contrast, the amount by which a starburst fades is directly proportional to its duration τ_{SB} (see eq. [39]), which might a priori be expected to vary significantly from system to system. It is unclear what would cause such a narrow range in τ_{SB} . It is, however, encouraging that the dynamical timescale at $\sim R_D$ is independent of the mass (σ) of a galaxy (eq. [8]), suggesting that to first order the duration of a merger-induced starburst might be similar in different systems.¹² It is also possible, as we discuss in the next section, that a central AGN is responsible for terminating the star formation in its host galaxy.

5. ACTIVE GALACTIC NUCLEI AND THE $M_{\text{BH}}-\sigma$ RELATION

Early-type galaxies and bulges are inferred to have central supermassive BHs, whose masses correlate well with the velocity dispersion of the galaxy itself: $M_{\text{BH}} = 1.5 \times 10^8 \sigma_{200}^4 M_{\odot}$ (Tremaine et al. 2002). This correlation is remarkably similar to the FJ relation.

In § 2.2 we considered the general properties of galactic winds driven by momentum deposition. We then focused on radiation from starbursts as providing this source of momentum. However, star formation is unlikely to efficiently remove gas from very small scales in galactic nuclei (scales much smaller than that of a nuclear starburst). This gas is available to fuel a central AGN.

We consider a central BH with a luminosity L_{BH} . The optically thin Eddington luminosity for the BH is (eq. [25])

$$L_{\text{Edd}} = \frac{4\pi GM_{\text{BH}}c}{\kappa_{\text{es}}} = 1.3 \times 10^{46} M_8 \text{ ergs s}^{-1}, \quad (40)$$

where $M_8 = M_{\text{BH}}/10^8 M_{\odot}$ and $\kappa_{\text{es}} = 0.38 \text{ cm}^2 \text{ g}^{-1}$ is the electron scattering opacity. Note that the electron scattering opacity is appropriate close to the BH, at least out to the dust sublimation radius. The latter can be estimated by equating the absorbed flux with the radiated flux from dust grains:

$$R_{\text{sub}} = \sqrt{\frac{L_{\text{BH}}}{4\pi\sigma_{\text{SB}}T_{\text{sub}}^4}} \sim 3 \times 10^{18} L_{46}^{1/2} \left(\frac{1200 \text{ K}}{T_{\text{sub}}} \right)^2 \text{ cm}, \quad (41)$$

¹¹ The timescale τ_{SB} refers to the net timescale over which stars form at a luminosity $\sim L_M$. It could in principle be that many starbursts of shorter duration cumulatively last for $\sim \tau_{\text{SB}}$.

¹² In numerical simulations of mergers, the duration of a starburst depends on the details of the orbit and the internal dynamics of the merger constituents (e.g., the bulge-to-disk ratio; see Mihos & Hernquist 1996). Variations in these properties from merger to merger will introduce scatter into τ_{SB} and thus the observed FJ relation.

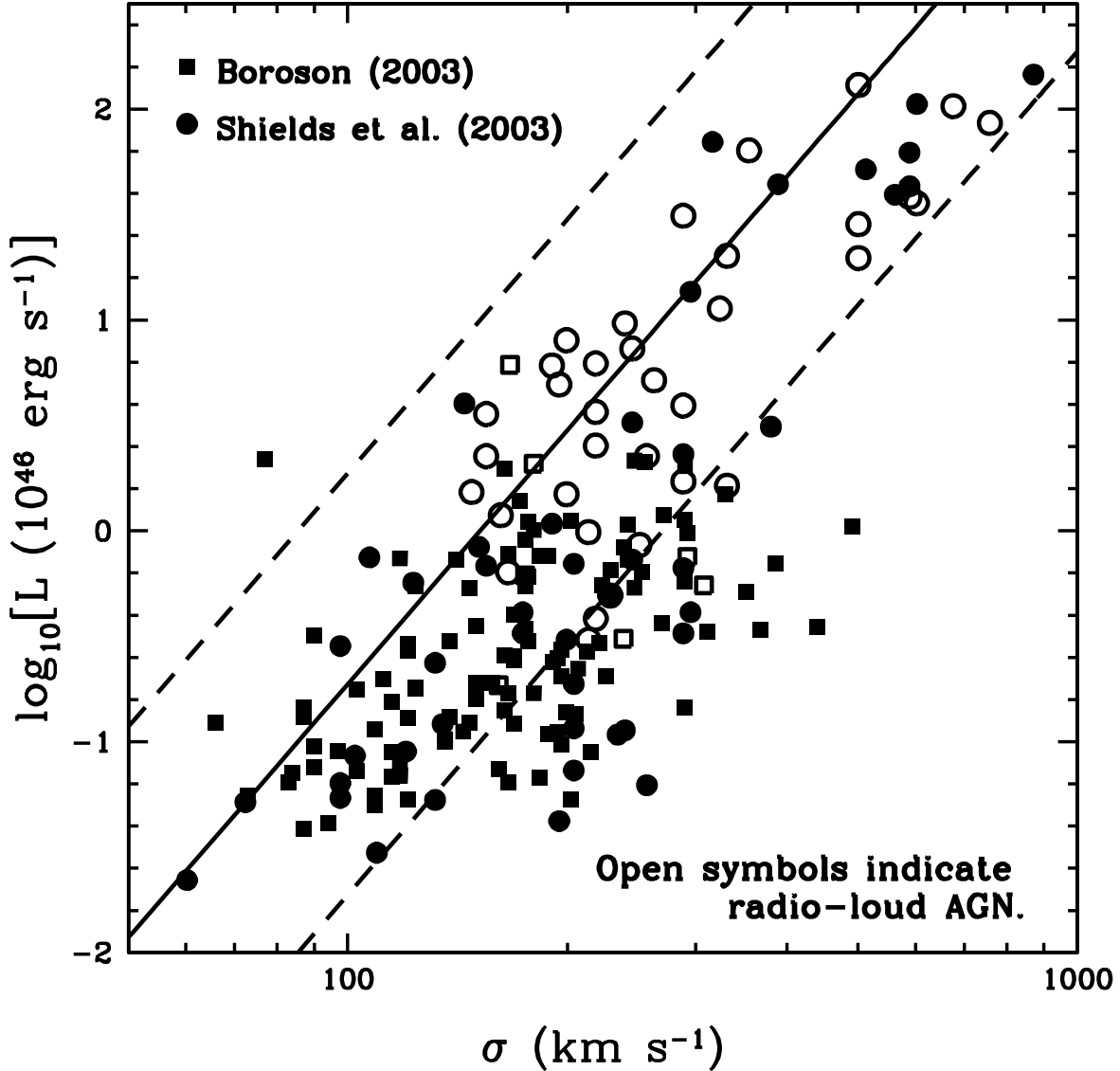


FIG. 4.—Same as Fig. 2, but for quasars from the SDSS sample of Boroson (2003; *squares*) and the compilation of Shields et al. (2003; *circles*). The velocity dispersion is estimated from the O III line width, while the luminosity is estimated using $L \approx 9\nu L_\nu(5100 \text{ \AA})$, the bolometric correction advocated by Kaspi et al. (2000). The limiting luminosity for momentum-driven galactic winds (L_M ; eq. [15]) is also shown, for three values of the gas fraction ($f_g = 0.1$, *thick solid line*; $f_g = 1.0$ and 0.01 , *dashed lines*). This limit accounts reasonably well for the maximum quasar luminosity at any σ . Note that Boroson (2003) does not present his observed values of $\nu L_\nu(5100 \text{ \AA})$, but they can be determined from his inferred BH masses and H β line widths ($v_{H\beta}$) using $M_{\text{BH}} = 3v_{H\beta}^2 R_{\text{BLR}}/(4G)$ and $R_{\text{BLR}} = 34[\nu L_\nu(5100 \text{ \AA})/10^{44} \text{ ergs s}^{-1}]^{0.7} \text{ lt-days}$, where R_{BLR} is the radius of the broad-line region (see his Table 1). [See the electronic edition of the Journal for a color version of this figure.]

where $L_{46} = L_{\text{BH}}/10^{46} \text{ ergs s}^{-1}$, σ_{SB} is the Stefan-Boltzmann constant, and the dust sublimation temperature is $T_{\text{sub}} \approx 1200 \text{ K}$.

The ratio $\Gamma \equiv L_{\text{BH}}/L_{\text{Edd}}$ is estimated to be ~ 0.1 – 1 for luminous AGNs at high redshift (e.g., Vestergaard 2004). If the hole radiates with an efficiency $\eta \approx 0.1$, the mass accretion rate is $\dot{M}_{\text{BH}} = L_{\text{BH}}/(\eta c^2)$. Combining \dot{M}_{BH} and L_{Edd} gives the timescale for L_{BH} (and M_{BH}) to double, the Salpeter timescale,

$$\tau_{\text{Salp}} = \frac{\eta c \kappa_{\text{es}}}{\Gamma 4\pi G} \sim 43 \Gamma^{-1} \text{ Myr}. \quad (42)$$

The region exterior to the sublimation radius contains dust and can be optically thick to the UV photons of the AGN even if the AGN is sub-Eddington in the electron scattering sense (eq. [40]). This is simply because the dust opacity is much larger than the electron scattering opacity. Thus, by arguments analogous to those given in §§ 2.2 and 4, if the luminosity of the

BH exceeds L_M (eq. [15]), it drives an outflow. This outflow drives away gas outside of R_{sub} , irrespective of whether or not the AGN is super-Eddington on small scales close to the BH.

Using $L_{\text{BH}} = \Gamma L_{\text{Edd}}$, the criterion $L_{\text{BH}} \approx L_M$ can be written in terms of the BH mass as

$$M_{\text{BH}} \approx \frac{f_g \kappa_{\text{es}}}{\pi G^2 \Gamma} \sigma^4 \approx 2 \times 10^8 f_{g,0.1} \Gamma^{-1} \sigma_{200}^4 M_\odot. \quad (43)$$

If the BH mass exceeds the limit in equation (43), then it drives a large-scale galactic outflow. Only when M_{BH} reaches the critical mass in equation (43) will it be able to blow dusty gas all the way out of the galaxy. This shuts off the gas supply to the BH on a dynamical timescale and fixes the mass to be that in equation (43), in good agreement with the observed M_{BH} – σ relation. It should be noted that the dust-free gas within R_{sub} need not be blown out by the BH. The total mass contained

within this region is, however, a small fraction (roughly a few percent) of the BH mass (eq. [43]), so accretion of this gas does not modify the $M_{\text{BH}}-\sigma$ relation.

Although the context is somewhat different, equation (43) is identical to the $M_{\text{BH}}-\sigma$ relation derived by King (2003) and is similar to those obtained using other “feedback” arguments for the $M_{\text{BH}}-\sigma$ relation (e.g., Silk & Rees 1998; Haehnelt et al. 1998; Blandford 1999; Fabian 1999; Fabian et al. 2002). Specifically, King assumed that a radiation pressure–driven outflow launched from close to the BH sweeps out of the galaxy, driving all of the gas away. We argue that the outflow is primarily due to absorption of the BH luminosity by dust outside of R_{sub} , independent of whether or not the AGN drives an outflow from small radii $\ll R_{\text{sub}}$.

An interesting feature of our model, or, more generally, of observations of AGNs and starbursts, is the apparent coincidence that the Salpeter time that governs the growth of the BH is comparable to the duration of the star formation epoch (see § 4 for a discussion of the latter). Were the Salpeter time much shorter, the BH would grow rapidly and its outflows could significantly disrupt star formation before sufficient stars formed to lie on the FJ relation. As is, we suggest that both the star formation and BH growth are independently self-regulating, reaching the maximum luminosity $\sim L_M$ (eq. [15]). However, as explained in the previous section, it is unclear what determines the duration of the star formation epoch. This may be determined by mergers, but it is also possible that the “coincidence” between τ_{Salp} and τ_{SB} is no coincidence at all: when the BH reaches the mass given in equation (43), it drives an outflow that sweeps out from the galactic nucleus, terminating star formation in its host galaxy (e.g., Silk & Rees 1998; Fabian 1999). This possibility is interesting because the Salpeter time is likely to be similar in different systems, which could explain the narrow range of τ_{SB} required to understand the FJ relation.

The above discussion assumes that BHs reach, but do not significantly exceed, the luminosity L_M . In Figure 4 we test this prediction using data compiled by Boroson (2003) and Shields et al. (2003). Both papers estimate the velocity dispersion of galaxies hosting quasars using the width of the narrow O III line (see Nelson 2000). The bolometric luminosity is estimated using $L \approx 9\nu L_\nu(5100 \text{ \AA})$, the average bolometric correction used by Kaspi et al. (2000). There is evidence that the width of the O III line can sometimes exceed the velocity dispersion of the galaxy in radio-loud AGNs (Nelson & Whittle 1996); these systems are indicated by open symbols in Figure 4.

Figure 4 shows that the limit L_M accounts for the maximum quasar luminosity at any σ , in good agreement with the predictions of feedback models for the $M_{\text{BH}}-\sigma$ relation. That some systems lie below L_M is not surprising because most BHs spend most of their time accreting at sub-Eddington rates; note also that Boroson's sample from SDSS contains only quasars with $z \lesssim 0.5$ and thus systematically lacks high-redshift, high-luminosity quasars.

6. DISCUSSION

6.1. Galactic Winds

In this paper we have investigated large-scale galactic winds driven by momentum deposition, in contrast to the usual assumption that energy deposition (thermal heating) by core-collapse SNe drives these outflows. The efficiency of energy-driven outflows is uncertain because much of the energy deposited by SNe in the ISM may be radiated away. Even in this limit, momentum injection by SNe is important and can itself generate a powerful outflow. SNe contribute to momentum

driving in a second way: the dynamics of cold gas entrained in a hot flow is analogous to that of a momentum-driven wind (see § 3.1 and the Appendix). Note that these mechanisms are physically distinct. The latter (ram pressure driving of cold gas) requires a powerful hot wind, while the former operates even if the SN energy is radiated away.

In addition to SNe, momentum injection is provided by continuum absorption and scattering of radiation on dust grains (radiation pressure); such radiation can be produced by either a starburst or a central AGN (or both) and is an efficient mechanism for driving cold, dusty gas out of a galaxy. Interestingly, the forces due to radiation pressure and ram pressure (entrainment) may be comparable in many cases (see eq. [A1]). Distinguishing which mechanism dominates is nontrivial. One way may be to assess the mass-loss rate in hot gas via X-ray observations (see, however, Strickland & Stevens [2000], who argue that such observations do not necessarily probe the energy-containing phase of the hot wind).

Although uncertain, we suggest that momentum injection may be more effective at halting star formation and blowing away the gas in a galaxy than energy injection. For example, SN energy can be efficiently vented by blowing out of the galactic disk, even if little of the mass is lost (De Young & Heckman 1994). By contrast, the momentum of SN explosions cannot be similarly vented and thus may be more disruptive to the bulk of the gas in a galaxy. In addition, because the mass of a galaxy is primarily in the cold phase, radiation pressure and ram pressure driving of cold gas may dominate the mass loss in starbursting galaxies (even in the presence of a hot thermal wind).

Momentum-driven winds have several properties that may allow them to be distinguished from energy-driven winds (§ 2.2). Specifically, (1) the momentum flux in the outflow, $\dot{M}_W V_\infty$, is comparable to that in the radiation field, L/c (eq. [12]), and (2) the terminal velocity of the outflow should be comparable to the velocity dispersion of the host galaxy, $V_\infty \sim \sigma$ (eqs. [17] and [26]). Note that these predictions apply to outflowing cold gas driven by momentum deposition. The hot thermally driven phase of a galactic wind satisfies different scalings (see § 3).

The simple predictions above for mass-loss rates and terminal velocities could be readily incorporated into cosmological simulations to assess the global impact of momentum-driven galactic winds (as in the work of Aguirre et al. 2001b). One interesting possibility is that because the energy carried by a momentum-driven wind may be smaller than that of a thermal SN-driven wind,¹³ momentum-driven winds may pollute the IGM with metals without significantly modifying its structure from that predicted by the gravitational instability paradigm.

6.2. The Growth of Elliptical Galaxies and Black Holes

In addition to considering the general properties of momentum-driven galactic winds, we have derived a limiting luminosity, $L_M \simeq (4f_g c/G)\sigma^4$, above which momentum deposition is sufficient to drive away a significant fraction of the gas in a galaxy (eq. [15]; King [2003] derived a similar result in the context of BH growth; Meurer et al. [1997] and Lehnert & Heckman [1996] discuss a potentially related observational limit on the surface brightness of local and high- z starburst galaxies). This outflow may regulate star formation during the formation of elliptical galaxies at high redshift by limiting the gas available for star formation, ensuring that the luminosity never significantly exceeds L_M . The fact that massive starbursts

¹³ The energy carried by a momentum-driven wind is $\sim V_\infty L/c \sim \sigma L/c$, while that in a thermal SN-driven wind is $\sim 10^{-2} \xi L$.

have luminosities near L_M (Fig. 2; § 4) and that starbursts at $z \gtrsim 1$ account for a significant fraction of the local stellar inventory (e.g., Madau et al. 1998) supports a model in which, during the hierarchical growth of galaxies, mergers trigger intense starbursts ($L \sim L_M$) that form a significant fraction of the stars in early-type galaxies.

We have focused on the growth of elliptical galaxies, rather than spiral galaxies, because there is evidence that star formation in spiral galaxies is reasonably quiescent (e.g., Kennicutt et al. 1994) and it is thus unlikely that a significant fraction of the mass in spiral galaxies was formed during bursts that reached our limiting luminosity L_M . By contrast, elliptical galaxies are inferred to have formed most of their stars relatively quickly at high redshift $\gtrsim 1-3$ (e.g., van Dokkum et al. 2004).

Our hypothesis that protoelliptical galaxies at high redshift go through an extended period of star formation with $L \sim L_M \propto \sigma^4$ can explain the FJ relation between the *current* luminosity and velocity dispersion of elliptical galaxies (§ 4.2). Specifically, our model explains quantitatively why elliptical galaxies do not have $L \propto M_{\text{DM}} \propto \sigma^3$ (where M_{DM} is the total mass of the dark matter halo), as would be expected if a fixed fraction of the available gas were converted into stars. Our model also explains why elliptical galaxies do not have $L \propto \sigma^5$, which would be expected if energy deposition from SNe dominated feedback (Fig. 1). Since the luminosity of a starburst is dominated by the rate at which high-mass stars are being formed, while the current luminosity of elliptical galaxies (reflected in FJ) depends on the total number of low-mass stars in the galaxy, our interpretation of FJ requires that the duration of peak star formation activity was relatively similar in different galaxies (so that both the peak star formation rate and the total number of stars formed are similar).¹⁴ By comparing the limiting luminosity L_M with the current FJ relation, we infer a star formation duration of $\sim 100-300$ Myr (§ 4.2). This is in reasonable agreement with observational inferences in LBGs (e.g., Shapley et al. 2001) and ULIRGs (e.g., Genzel et al. 2004).

Our model for the origin of the FJ relation does not fully explain why elliptical galaxies lie in the fundamental plane. Roughly speaking, the fundamental plane can be understood via two projections: $L \propto \sigma^4$ (the FJ relation) and $R_{\text{eff}} \propto \sigma^{8/3}$, where R_{eff} is the effective radius (Bernardi et al. 2003). The latter relation is very different from any virial prediction, which would suggest $R_{\text{eff}} \propto \sigma$, and its origin, whether a consequence of gas physics or collisionless mergers of stellar systems, is unknown.

Unlike elliptical galaxies, the optical Tully-Fisher relation in spiral galaxies is reasonably consistent with $L \propto v_c^3$ (where v_c is the maximum circular velocity; e.g., Giovanelli et al. 1997). This is probably a consequence of the more quiescent star formation histories of spiral galaxies (Kennicutt et al. 1994) so that feedback is less severe and the luminosity of a galaxy is simply proportional to its mass. However, the slope of the TF relation varies systematically with wavelength and in the IR, $L \propto v_c^4$ (e.g., Pierini & Tuffs 1999), consistent with the FJ scaling for elliptical galaxies. This is very intriguing and might suggest that the oldest stars in spiral galaxies were formed in bursts analogous to those that formed elliptical galaxies.

6.2.1. Black Holes

In addition to considering the self-regulated growth of elliptical galaxies via starbursts, we propose that the growth of

BHs in early-type galaxies proceeds in a similar manner. As a BH grows via accretion, its luminosity may eventually exceed $\sim L_M$. When it does so, the dusty gas around the BH (outside the sublimation radius; eq. [41]) is blown away by radiation pressure. The BH thus shuts off its own fuel supply. This fixes the BH mass to lie very close to the observationally inferred $M_{\text{BH}}-\sigma$ relation (see eq. [43]). If star formation in the host galaxy is still ongoing when the BH reaches $\sim L_M$, the outflow from the galactic nucleus may sweep through the galaxy, terminating star formation. This possibility is interesting because it may explain the apparent coincidence that the Salpeter time characterizing the growth of BHs (eq. [42]) is similar to the inferred duration of star formation in high-redshift starbursts (see §§ 4 and 5).

Previous discussions of the interaction between a central BH and its surrounding galaxy have also emphasized how the central BH can regulate its own fuel supply by driving away ambient gas (e.g., Silk & Rees 1998; Haehnelt et al. 1998; Blandford 1999; Fabian 1999; King 2003). All such models are broadly similar (ours included), although they differ in detail as to whether energy deposition or momentum deposition is the most important feedback mechanism. However, implicit in previous discussions of the $M_{\text{BH}}-\sigma$ relation is that the stars in the galaxy “know” when the hole is about to reach the limiting mass at which it can blow away the surrounding gas. Otherwise, it is unclear how the right number of stars are formed so that the galaxy lies on the FJ relation. One explanation for this is to hypothesize that the stars form as the gas is being blown out by the AGN, i.e., in one dynamical time (e.g., King 2003). Observationally, however, this is not the case in either LBGs or ULIRGs, where the star formation lasts for hundreds of millions of years. Instead, we argue that the AGN’s role may be subdominant: feedback from stars determines the maximal luminosity of a starburst, whether or not there is an AGN present. It is, however, possible that the AGN administers the coup de grâce, terminating star formation.

In our interpretation, the peak episode of star formation likely precedes that of AGN activity in most galaxies. There are two reasons for this. First, gas is transported from the outside in. Therefore, star formation on galactic scales sets in before the central BH is fed. Second, if the BH were to grow and reach the $M_{\text{BH}}-\sigma$ relation *before* significant star formation has occurred, it will blow out the ambient gas in the galaxy before the FJ relation is set. If the galaxy were to later accrete gas, from the IGM or via a merger, because the BH is already on the $M_{\text{BH}}-\sigma$ relation, even a small amount of accretion onto the BH would be sufficient to again disrupt star formation. There is some observational support for this temporal ordering. First, the number density of bright quasars declines more rapidly at high z than the number density of star-forming galaxies (compare Fan et al. 2004 and Heavens et al. 2004). Second, although some rapidly star-forming SCUBA sources at high z are inferred to host quasars, in many cases there is X-ray evidence for more modest AGNs with $L \sim 10^{43}-10^{44}$ ergs s^{-1} (e.g., Alexander et al. 2003). Since many of the observed systems are Compton thin, it is unlikely that a quasar-like luminosity is hidden by obscuration. Given the inferred $\sigma \sim 200-300$ km s^{-1} in the SCUBA sources (§ 4 and Table 1), BHs on the $M_{\text{BH}}-\sigma$ relation would have $M \sim 10^8-10^9 M_\odot$. To explain the observed luminosities would then require substantially sub-Eddington accretion rates. While possible, this would be surprising in view of the large available gas supply. It is perhaps more plausible that the BH is still growing and has not yet reached the $M_{\text{BH}}-\sigma$ relation (e.g., Archibald et al. 2002).

¹⁴ Note that this will be a requirement for any model that tries to explain the FJ relation as a result of feedback during starbursts because feedback (generically defined) is sensitive to the star formation rate, rather than the total number of stars formed.

Our model makes the very strong prediction that the peak luminosity of star formation and AGN activity in a given galaxy are essentially the same ($\sim L_M$), set by the criterion that a momentum-driven outflow blows away gas that would otherwise be available for star formation/accretion. Figures 2 and 4 provide observational evidence that is consistent with this prediction.

We note, however, that in order to reach a luminosity $\sim L_M$, a galaxy with $\sigma = 200\sigma_{200}$ km s $^{-1}$ must have a star formation rate of $\approx 500\sigma_{200}^4 M_\odot$ yr $^{-1}$ (eq. [19]), while a BH must accrete gas at $\approx 5\sigma_{200}^4 M_\odot$ yr $^{-1}$. Moreover, if the most luminous observed AGNs ($L \sim 10^{48}$ ergs s $^{-1}$; see Fig. 4) are Eddington limited and lie on the $M_{\text{BH}}-\sigma$ relation, then their host galaxies must have $\sigma \sim 500$ km s $^{-1}$. If such galaxies indeed exist and if star formation is to reach a luminosity $\sim L_M$, then the required star formation rate is $\sim 10^4 M_\odot$ yr $^{-1}$! Such a starburst has never been observed but would of course be extremely rare. It is unclear whether such a star formation rate can actually be achieved and sustained. If not, then we predict deviations from the FJ relation for the largest elliptical galaxies ($\sigma > \sigma_{\text{max}}$; see Fig. 1).

We thank Crystal Martin for an inspiring talk that motivated this work and for useful conversations. We also thank Alice Shapley, Leo Blitz, Martin White, James Graham, Avishai Dekel, Reinhard Genzel, Anthony Aguirre, Chung-Pei Ma, Yoram Lithwick, Volker Springel, and Jon Arons for helpful conversations. We thank A. Bruzual, S. Charlot, and C. Leitherer for making their starburst models available and Gabriela Mallén-Ornelas for providing us with data from her thesis. We thank the referee for useful comments. N. M. is supported in part by the Canada Research Chair program and the Miller Foundation. N. M. extends his gratitude to the University of California at Berkeley where much of this work was completed. T. A. T. is supported by NASA through Hubble Fellowship grant HST-HF-01157.01-A awarded by the Space Telescope Science Institute, which is operated by the Association of Universities for Research in Astronomy, Inc., for NASA, under contract NAS 5-26555. E. Q. is supported in part by NSF grant AST 02-06006, NASA grant NAG5-12043, an Alfred P. Sloan Fellowship, and the David and Lucile Packard Foundation.

APPENDIX

ENERGY-DRIVEN GALACTIC WINDS: ENTRAINMENT

In this appendix we consider entrainment in two limits: (1) entrainment of individual clouds (the “optically thin” limit) and (2) entrainment of shells of gas (the “optically thick” limit, appropriate when the cold gas occupies a large fraction of 4π sr on the sky and thus intercepts much of the momentum flux in the hot flow). We show that in both limits the dynamics of cold gas entrained in a hot flow is analogous to that of the momentum-driven winds considered in § 2.2.

A1. ENTRAINMENT: THE “OPTICALLY THIN” LIMIT

We first consider the entrainment of individual clouds of cold gas; the clouds have projected area A_c , density ρ_c , and mass $M_c = (4\pi/3)\rho_c R_c^3 = (4/3)A_c R_c \rho_c$. The hot wind has a density $\rho_h = \dot{M}_h / (4\pi r^2 V_h)$, a mass-loss rate \dot{M}_h , and a velocity V_h .¹⁵ The ram pressure force on a cold cloud is $\rho_h V_h^2 A_c$. Comparing this to the radiation pressure force on the cloud (assuming that it is optically thick to radiation) yields

$$\frac{F_{\text{ram}}}{F_{\text{rad}}} = \frac{\rho_h V_h^2 A_c}{(L/c)(A_c/4\pi r^2)} = \left(\frac{\dot{M}_h}{\dot{M}_*}\right) \left(\frac{V_h}{300\epsilon_3 \text{ km s}^{-1}}\right) \approx \frac{600\xi_{0.1} \text{ km s}^{-1}}{V_h}, \quad (\text{A1})$$

where $A_c/(4\pi r^2)$ is the fraction of photons intercepted by the cloud and in the last equality we used $\dot{E}_{\text{SN}} = \frac{1}{2}\dot{M}_h V_h^2 = 10^{-2}\xi L$. Equation (A1) shows that ram pressure and radiation pressure can contribute comparably to the driving of cold gas, so long as $\dot{M}_h \sim \dot{M}_*$. Shocked SN ejecta contribute a total mass loss of $\sim 0.1\dot{M}_*$ in the absence of radiative cooling. It is, however, plausible that considerable swept-up mass is also shock heated, leading to $\dot{M}_h \sim \dot{M}_*$ (see, e.g., Martin 1999 for evidence to this effect in local starbursts). Note that $V_h \sim 300\text{--}600$ km s $^{-1}$ is consistent with the observed temperature of hot outflowing gas in local starbursts (e.g., Martin 1999).

In the limit that ram pressure dominates the driving of cold gas, we can derive the velocity of the cloud as a function of distance from the galaxy by analogy with the optically thin radiation pressure limit considered in § 2.2 (since $F_{\text{ram}} = \rho_h V_h^2 A_c \propto r^{-2}$, the optically thin limit, rather than the optically thick limit, is the appropriate analogy). The velocity profile is given by

$$V(r) = \sqrt{V_c^2 \left(\frac{1-R_0}{r}\right) - 4\sigma^2 \ln\left(\frac{r}{R_0}\right)}, \quad (\text{A2})$$

where R_0 is the initial “launching” radius and

$$V_c^2 = 3 \frac{\dot{M}_h V_h}{8\pi\rho_c R_c R_0}. \quad (\text{A3})$$

The velocity V_c is the characteristic velocity the cloud reaches before it begins to decelerate in the extended gravitational potential of the galaxy. Note that equation (A3) is only appropriate for $V_c < V_h$; if equation (A3) predicts $V_c > V_h$, the actual maximal velocity is V_h since ram pressure ceases to accelerate the cloud above this velocity.

¹⁵ In this section we use the subscript “h” for “hot,” rather than our previous subscript “W” for “wind,” to emphasize that these mass-loss rates and velocities refer to those of the hot flow.

In order for the cloud to move to a radius significantly larger than its starting position at $\sim R_0$, we require $V_c \gtrsim 2\sigma$. Using $\rho_c R_c = m_p N_H$, this requirement can be rewritten as

$$\dot{M}_h \gtrsim \frac{32\pi\sigma^2 m_p N_H R_0}{3V_h} \approx 35 \sigma_{200}^2 N_{21} \left(\frac{R_0}{1 \text{ kpc}} \right) \left(\frac{300 \text{ km s}^{-1}}{V_h} \right) M_\odot \text{ yr}^{-1}. \quad (\text{A4})$$

If \dot{M}_h is less than the value given in equation (A4), cold clouds cannot be pushed out of the nuclear region by the hot flow. This criterion is analogous to the optically thin Eddington limit given in equation (28). Indeed, if $\dot{M}_h \approx \dot{M}_*$, then $F_{\text{ram}} \approx F_{\text{rad}}$ (eq. [A1]) and so the two ‘‘Eddington limits’’ are essentially equivalent.

The cloud velocity V_c can be rewritten as

$$\frac{V_c}{V_h} = \sqrt{\frac{3\dot{M}_h}{8\pi m_p N_H V_h R_0}} \approx \left[\left(\frac{\dot{M}_h}{10 M_\odot \text{ yr}^{-1}} \right) \left(\frac{10^{21} \text{ cm}^2}{N_H} \right) \left(\frac{1 \text{ kpc}}{R_0} \right) \left(\frac{300 \text{ km s}^{-1}}{V_h} \right) \right]^{1/2}. \quad (\text{A5})$$

Equation (A5) implies that, for clouds of a given column N_H , there is a critical mass-loss rate $\sim 10 M_\odot \text{ yr}^{-1}$ (in the hot phase) below which ram pressure is insufficient to accelerate clouds of cold material to a velocity $\sim V_h$, i.e., to the velocity of the hot wind. Assuming that $\dot{M}_h \sim \dot{M}_*$, this can be equivalently interpreted as defining a critical star formation rate $\dot{M}_c \sim 10 M_\odot \text{ yr}^{-1}$ such that for $\dot{M}_* \gtrsim \dot{M}_c$, $V_c \approx V_h$. However, if $\dot{M}_* \lesssim \dot{M}_c$, then $V_c \lesssim V_h$ with $V_c \propto [\dot{M}_*/(N_H R_0)]^{1/2}$. Note that the precise value of \dot{M}_c is uncertain because it depends on the column N_H and the launching radius R_0 .

2. ENTRAINMENT: THE ‘‘OPTICALLY THICK’’ LIMIT

If the cold gas covers a significant fraction of the sky, it will intercept most of the momentum flux in the hot flow. The ram pressure force on the cold gas is then given by $\rho_h v_h^2 4\pi r^2$, rather than $\rho_h v_h^2 A_c$ as considered in the previous section. We call this the ‘‘optically thick’’ limit. In this limit, the requirement to blow out all of the cold gas in the galaxy by ram pressure is that

$$\rho_h v_h^2 4\pi r^2 \gtrsim \frac{G M M_g}{r^2} \approx \frac{4f_g \sigma^4}{G}, \quad (\text{A6})$$

where we assume that most of the mass M_g is in the cold phase. Equation (A6) can be rewritten as a requirement on the luminosity of the starburst as follows: we rewrite ρ_h in terms of \dot{M}_h and then use $\dot{E}_{\text{SN}} = \frac{1}{2} \dot{M}_h v_h^2 = 10^{-2} \xi L$ to find

$$L \gtrsim L_M^{\text{ent}} \equiv \frac{4f_g c}{G} \sigma^4 \left(\frac{V_h}{600 \xi_{0.1} \text{ km s}^{-1}} \right). \quad (\text{A7})$$

Equation (A7) is essentially the same as equation (15), the criterion to blow away all of the gas via a momentum-driven wind.

Note, however, that the normalization in equation (A7) depends on ξ , the efficiency with which SN energy is thermalized in the ISM. For our fiducial value of $\xi \approx 0.1$, $L_M^{\text{ent}} \approx L_M$, i.e., the limits set by ram pressure and radiation pressure driving are comparable. By contrast, if $\xi \sim 1$, ram pressure dominates, while if $\xi \lesssim 0.1$, radiation pressure dominates.

REFERENCES

- Abbott, D. C. 1982, *ApJ*, 263, 723
 Adelberger, K. L., & Steidel, C. C. 2000, *ApJ*, 544, 218
 Adelberger, K. L., Steidel, C. C., Shapley, A. E., & Pettini, M. 2003, *ApJ*, 584, 45
 Aguirre, A. 1999, *ApJ*, 525, 583
 Aguirre, A., Hernquist, L., Katz, N., Gardner, J., & Weinberg, D. 2001a, *ApJ*, 556, L11
 Aguirre, A., Hernquist, L., Schaye, J., Katz, N., Weinberg, D. H., & Gardner, J. 2001b, *ApJ*, 561, 521
 Aguirre, A., Hernquist, L., Schaye, J., Weinberg, D. H., Katz, N., & Gardner, J. 2001c, *ApJ*, 560, 599
 Alexander, D. M., et al. 2003, *AJ*, 125, 383
 Archibald, E. N., Dunlop, J. S., Jimenez, R., Friaça, A. C. S., McLure, R. J., & Hughes, D. H. 2002, *MNRAS*, 336, 353
 Bernardi, M., et al. 2003, *AJ*, 125, 1849
 Binney, J., & Merrifield, M. 1998, *Galactic Astronomy* (Princeton: Princeton Univ. Press)
 Blandford, R. D. 1999, in *ASP Conf. Ser. 182, Galaxy Dynamics*, ed. D. R. Merritt, M. Valluri, & J. A. Sellwood (San Francisco: ASP), 87
 Boroson, T. A. 2003, *ApJ*, 585, 647
 Bruzual, A. G., & Charlot, S. 2003, *MNRAS*, 344, 1000
 Bullock, J. S., Dekel, A., Kolatt, T. S., Kravtsov, A. V., Klypin, A. A., Porciani, C., & Primack, J. R. 2001, *ApJ*, 555, 240
 Burstein, D., Bender, R., Faber, S., & Nolthenius, R. 1997, *AJ*, 114, 1365
 Calzetti, D. 2001, *PASP*, 113, 1449
 Chevalier, R. A., & Clegg, A. W. 1985, *Nature*, 317, 44
 Davies, J. I., Alton, P., Bianchi, S., & Trewella, M. 1998, *MNRAS*, 300, 1006
 Dekel, A., & Silk, J. 1986, *ApJ*, 303, 39
 De Young, D. S., & Heckman, T. M. 1994, *ApJ*, 431, 598
 Draine, B. T., & Lee, H. M. 1984, *ApJ*, 285, 89
 Draine, B. T., & Salpeter, E. E. 1979, *ApJ*, 231, 77
 Elmegreen, B. G. 1983, *MNRAS*, 203, 1011
 Erb, D. K., Shapley, A. E., Steidel, C. C., Pettini, M., Adelberger, K. L., Hunt, M. P., Moorwood, A. F. M., & Cuby, J. 2003, *ApJ*, 591, 101
 Faber, S. M., & Jackson, R. E. 1976, *ApJ*, 204, 668
 Fabian, A. C. 1999, *MNRAS*, 308, L39
 Fabian, A. C., Wilman, R. J., & Crawford, C. S. 2002, *MNRAS*, 329, L18
 Fan, X., et al. 2004, *AJ*, 128, 515
 Ferrarese, L., & Merritt, D. 2000, *ApJ*, 539, L9
 Gebhardt, K., et al. 2000, *ApJ*, 539, L13
 Genzel, R., Baker, A. J., Tacconi, L. J., Lutz, D., Cox, P., Guilleaume, S., & Omont, A. 2003, *ApJ*, 584, 633
 Genzel, R., & Cesarsky, C. J. 2000, *ARA&A*, 38, 761
 Genzel, R., Tacconi, L. J., Rigopoulou, D., Lutz, D., & Tecza, M. 2001, *ApJ*, 563, 527
 Genzel, R., et al. 2004, in *Multiwavelength Mapping of Galaxy Formation and Evolution*, in press (astro-ph/0403183)
 Giovanelli, R., Haynes, M. P., da Costa, L. N., Freudling, W., Salzer, J. J., & Wegner, G. 1997, *ApJ*, 477, L1
 Haehnelt, M. G. 1995, *MNRAS*, 273, 249
 Haehnelt, M. G., Natarajan, P., & Rees, M. J. 1998, *MNRAS*, 300, 817
 Heavens, A., Panter, B., Jimenez, R., & Dunlop, J. 2004, *Nature*, 428, 625
 Heckman, T. M. 2000, *Philos. Trans. R. Soc. London*, A358, 2077
 Heckman, T. M., Armus, L., & Miley, G. K. 1990, *ApJS*, 74, 833

- Heckman, T. M., Lehnert, M. D., Strickland, D. K., & Armus, L. 2000, *ApJS*, 129, 493
- Kaspi, S., Smith, P. S., Netzer, H., Maoz, D., Jannuzi, B. T., & Giveon, U. 2000, *ApJ*, 533, 631
- Kennicutt, R. C., Jr., Tamblyn, P., & Congdon, C. E. 1994, *ApJ*, 435, 22
- King, A. 2003, *ApJ*, 596, L27
- Klein, R. I., McKee, C. F., & Colella, P. 1994, *ApJ*, 420, 213
- Kozasa, T., Hasegawa, H., & Nomoto, K. 1989, *ApJ*, 344, 325
- Lehnert, M. D., & Heckman, T. M. 1996, *ApJ*, 472, 546
- Leitherer, C., et al. 1999, *ApJS*, 123, 3
- Lilly, S. J., Le Fevre, O., Hammer, F., & Crampton, D. 1996, *ApJ*, 460, L1
- Mac Low, M., & Ferrara, A. 1999, *ApJ*, 513, 142
- Madau, P., Ferguson, H. C., Dickinson, M. E., Giavalisco, M., Steidel, C. C., & Fruchter, A. 1996, *MNRAS*, 283, 1388
- Madau, P., Pozzetti, L., & Dickinson, M. 1998, *ApJ*, 498, 106
- Mallén-Ornelas, G., Lilly, S. J., Crampton, D., & Schade, D. 1999, *ApJ*, 518, L83
- Martin, C. L. 1998, *ApJ*, 506, 222
- . 1999, *ApJ*, 513, 156
- . 2004, *ApJ*, submitted (astro-ph/0410247)
- Mateo, M. 1998, *ARA&A*, 36, 435
- Melnick, J., Terlevich, R., & Moles, M. 1988, *MNRAS*, 235, 297
- Meurer, G. R., Heckman, T. M., Lehnert, M. D., Leitherer, C., & Lowenthal, J. 1997, *AJ*, 114, 54
- Meurer, G. R., Heckman, T. M., Leitherer, C., Kinney, A., Robert, C., & Garnett, D. R. 1995, *AJ*, 110, 2665
- Mihos, J. C., & Hernquist, L. 1996, *ApJ*, 464, 641
- Mo, H. J., Mao, S., & White, S. D. M. 1998, *MNRAS*, 295, 319
- Nelson, C. H. 2000, *ApJ*, 544, L91
- Nelson, C. H., & Whittle, M. 1996, *ApJ*, 465, 96
- Neri, R., et al. 2003, *ApJ*, 597, L113
- Netzer, N., & Elitzur, M. 1993, *ApJ*, 410, 701
- Nozawa, T., Kozasa, T., Umeda, H., Maeda, K., & Nomoto, K. 2003, *ApJ*, 598, 785
- Pahre, M. A., Djorgovski, S. G., & de Carvalho, R. R. 1998, *AJ*, 116, 1591
- Pettini, M., Shapley, A. E., Steidel, C. C., Cuby, J., Dickinson, M., Moorwood, A. F. M., Adelberger, K. L., & Giavalisco, M. 2001, *ApJ*, 554, 981
- Pettini, M., Steidel, C. C., Adelberger, K. L., Dickinson, M., & Giavalisco, M. 2000, *ApJ*, 528, 96
- Pierini, D., & Tuffs, R. J. 1999, *A&A*, 343, 751
- Poludnenko, A. Y., Frank, A., & Blackman, E. G. 2002, *ApJ*, 576, 832
- Sanders, D. B., & Mirabel, I. F. 1996, *ARA&A*, 34, 749
- Scoville, N. 2003, *J. Korean Astron. Soc.*, 36, 167
- Scoville, N., Polletta, M., Ewald, S., Stolovy, S., Thompson, R., & Rieke, M. 2001, *AJ*, 122, 3017
- Shapley, A. E., Steidel, C. C., Adelberger, K. L., Dickinson, M., Giavalisco, M., & Pettini, M. 2001, *ApJ*, 562, 95
- Shields, G. A., Gebhardt, K., Salviander, S., Wills, B. J., Xie, B., Brotherton, M. S., Yuan, J., & Dietrich, M. 2003, *ApJ*, 583, 124
- Silk, J., & Rees, M. J. 1998, *A&A*, 331, L1
- Smail, I., Ivison, R. J., & Blain, A. W. 1997, *ApJ*, 490, L5
- Steidel, C. C., Adelberger, K. L., Giavalisco, M., Dickinson, M., & Pettini, M. 1999, *ApJ*, 519, 1
- Steidel, C. C., Giavalisco, M., Pettini, M., Dickinson, M., & Adelberger, K. L. 1996, *ApJ*, 462, L17
- Strickland, D. K. 2004, in *IAU Symp. 222, The Interplay among Black Holes, Stars and ISM in Galactic Nuclei*, ed. Th. Storchi Bergmann, L. C. Ho, & H. R. Schmitt (San Francisco: ASP), in press (astro-ph/0404316)
- Strickland, D. K., & Stevens, I. R. 2000, *MNRAS*, 314, 511
- Tecza, M., et al. 2004, *ApJ*, 605, L109
- Telles, E., & Terlevich, R. 1997, *MNRAS*, 286, 183
- Thornton, K., Gaudlitz, M., Janka, H.-T., & Steinmetz, M. 1998, *ApJ*, 500, 95
- Todini, P., & Ferrara, A. 2001, *MNRAS*, 325, 726
- Tremaine, S., et al. 2002, *ApJ*, 574, 740
- van Dokkum, P. G., et al. 2004, *ApJ*, 611, 703
- Vestergaard, M. 2004, *ApJ*, 601, 676